Title: Maintenance of neuronal TDP-43 expression requires axonal lysosome transport

Authors: Veronica H. Ryan[1,2], Sydney Lawton[1], Joel F. Reyes[1], James Hawrot[1], Ashley M. Frankenfield[3], Sahba Seddighi[1], Daniel M. Ramos[2], Faraz Faghri[2,4], Nicholas L. Johnson[2,4], Jizhong Zou[5], Martin Kampmann[6], John Replogle[1], Hebao Yuan[1], Kory R. Johnson[1], Dragan Maric[1], Ling Hao[7], Mike A. Nalls[2,4], Michael E. Ward[1]

Affiliations
[1]National Institute of Neurological Disorders and Stroke, National Institutes of Health, Bethesda, MD, USA.
[2]Center for Alzheimer's and Related Dementias, National Institute on Aging, National Institutes of Health, Bethesda, MD, USA.
[3]Department of Chemistry, George Washington University, Washington, DC, USA.
[4]DataTecnica, Washington, DC, USA.
[5]National Heart, Lung, and Blood Institute, National Institutes of Health, Bethesda, MD, USA.
[6]Institute for Neurodegenerative Diseases, Weill Institute for Neurosciences, and Department of Biochemistry and Biophysics, University of California, San Francisco, San Francisco, CA, USA.
[7]Department of Chemistry and Biochemistry, University of Maryland, College Park, MD, USA.

Correspondence: michael.ward4@nih.gov and veronica.ryan@nih.gov

Abstract
TDP-43 mislocalization and pathology occurs across a range of neurodegenerative diseases, but the pathways that modulate TDP-43 in neurons are not well understood. We generated a Halo-TDP-43 knock-in iPSC line and performed a genome-wide CRISPR interference FACS-based screen to identify modifiers of TDP-43 levels in neurons. A meta-analysis of our screen and publicly available screens identified both specific hits and pathways present across multiple screens, the latter likely responsible for generic protein level maintenance. We identified BORC, a complex required for anterograde lysosome transport, as a specific modifier of TDP-43 protein, but not mRNA, levels in neurons. BORC loss led to longer half-life of TDP-43 and other proteins, suggesting lysosome location is required for proper protein turnover. As such, lysosome location and function are crucial for maintaining TDP-43 protein levels in neurons.

Introduction
Mislocalization of transactive response DNA binding protein of 43 kDa (TDP-43) is a pathological hallmark of frontotemporal dementia and amyotrophic lateral sclerosis (FTD/ALS), two related neurodegenerative diseases, and is a co-pathology in up to 57% of Alzheimer's disease cases[1]. Mislocalization of TDP-43 includes formation of aggregates in the cytosol and/or nucleus and nuclear clearance[2, 3]. TDP-43 plays important roles in the regulation of gene expression and is critical to mRNA splicing. Nuclear loss of TDP-43 leads to increased alternative splicing events, a hallmark of TDP-43 proteinopathies[4, 5]. TDP-43 also regulates its own expression at the mRNA levels by binding to its own 3' UTR, but this autoregulation is insufficient to maintain normal nuclear expression in disease[6-8]. Whether other factors also regulate TDP-43 expression in neurons has not been systematically studied. Identification of such factors could reveal upstream disease mechanisms and potential therapeutic targets for neurodegenerative diseases.

The development of pooled CRISPR interference (CRISPRi) screens has allowed researchers to test the effect of thousands of genetic perturbations in parallel[9]. CRISPRi screens are now possible in neurons derived from human induced pluripotent stem cells (iPSCs), enabling the evaluation of the effect of gene knockdowns on various phenotypes in these iPSC-derived

neurons (iNeurons). Initial screens in iNeurons focused on survival-related phenotypes[10, 11]. More recently, FACS-based screens in iNeurons have enabled identification of modifiers of oxidative stress and peroxidized lipids[11]. Historically, a practical challenge in the application of FACS-based screens to iNeurons has been that traditional genome-wide sgRNA libraries are large (>100K sgRNAs), making it difficult to sort sufficient cells to identify phenotypes. Therefore, sub-library screens have traditionally been used in the past, limiting the scope of genes assayed. Recently, compact dual-sgRNA CRISPRi libraries have been developed[12], setting the stage for genome-wide FACS-based screens in iNeurons.

To uncover mechanisms leading to altered TDP-43 protein levels, we endogenously tagged the TARDBP gene with HaloTag in iPSCs, thereby generating a Halo-TDP-43 knock-in iPSC line to monitor TDP-43 expression in iNeurons. Using this line, we conducted a whole genome CRISPRi FACS screen to identify modifiers of TDP-43 expression. Meta-analysis of this screen and previous CRISPRi screens revealed common pathways shared across screens independent of the measured phenotype, enabling us to rank pathways specific for TDP-43 expression. All eight of the components of the BORC complex, which is necessary for axonal lysosome transport[13], were required to maintain neuronal TDP-43 expression. The genes encoding the 8 subunits are BORCS1 (BLOC1S1), BORCS2 (BLOC1S2), BORCS3 (SNAPIN), BORCS4 (KXD1), BORCS5 (alias LOH1CR12), BORCS6 (alias C17orf59), BORCS7 (alias C10orf32), and BORCS8 (alias MEF2BNB). Knockdown of BORC reduced TDP-43 protein, but not RNA, levels. Surprisingly, metabolic labeling proteomics revealed that loss of BORC resulted in longer turnover time of TDP-43 protein. Notably, lysosome function and location also influenced Halo-TDP-43 levels in iNeurons. Our results identify BORC as a novel modifier of TDP-43 protein levels and point to a new mechanism by which TDP-43 levels are regulated in neurons.

Results

Generation of a Halo-TDP-43 knock in iPSC line

The amount of TDP-43 expressed in neurons is tightly regulated and TDP-43 undergoes autoregulation of its own transcript levels[14] to ensure levels are maintained at appropriate levels. To visualize and quantify the amount of TDP-43 in living cells, we used CRISPR technology to endogenously tag the N-terminus of TDP-43 with a HaloTag (Figure 1A). Gene editing was efficient, with almost all selected clones correctly edited. Sequencing of the targeted allele showed perfect overlap of the obtained sequence with the expected sequence. In the lead clone, knock in of the HaloTag was heterozygous, leaving the second allele of TDP-43 intact and unedited. The lead clone displayed a normal karyotype, demonstrating that there were no major chromosomal abnormalities introduced during the gene editing or subsequent clonal expansion (Figure S1A). Imaging of iNeurons differentiated from the knock in iPSC line showed the majority of Halo signal in the nucleus, as is expected for TDP-43 localization (Figure 1B). A western blot against TDP-43 shows a shift of approximately 35 kDa in the two TDP-43 positive bands, corresponding to the molecular weight of Halo (33 kDa) (Figure S1B, 1C). Knocking down TDP-43 using CRISPRi reduced the amount of both tagged and untagged TDP-43 (Figure 1C-D). Expression of Halo-TDP-43 was roughly 60% of endogenous TDP-43, indicating that the Halo-tagged protein is either not transcribed or translated as efficiently as untagged protein, or the protein is degraded more readily.

CRISPRi FACS screen identifies modifiers of Halo-TDP-43 levels in iPSC derived neurons

To identify upstream modifiers that either increase or decrease TDP-43 levels, we performed a genome-wide CRISPRi FACS-based screen in both Halo-TDP-43 iPSCs and iNeurons differentiated from our Halo-TDP-43 iPSC line using a dual sgRNA library, enabling 1000x coverage of the genome by sorting only 20 million iNeurons[12]. We sorted for cells highly

expressing the GFP sgRNA marker, and then sorted the cells containing the lowest 25% of halo signal into one tube and the cells containing the highest 25% of halo signal into another (Figure 2A). sgRNAs targeting the TARDBP transcription start site decreased Halo-TDP-43 levels in both the iPSC and iNeuron screens (Figure 2B and S2A), indicating that our screen successfully identified genes that decrease TDP-43 levels. Non-targeting guides are clustered in the middle of the rank plot for each screen, showing that gene knockdown is needed to alter Halo-TDP-43 levels (Figure 2B and S2A). For genes whose knockdown decreases Halo-TDP-43 levels, we identified all eight components of the BORC complex, which regulates anterograde lysosome transport in axons as hits in the iNeuron, but not iPSC screen (Figure 2B-C and S2A). Knockdown of genes related to mitochondrial function also decrease Halo-TDP-43 levels (Figure 2C and S2B). Further, we identified genes whose knockdown increases Halo-TDP-43 levels, including genes involved in RNA processing (Figure 2D and S2C). In comparing the top GO terms associated with genes that increase or decrease Halo-TDP-43 levels in iNeurons, we found that almost none altered Halo-TDP-43 levels in iPSCs, demonstrating that our hits are neuron specific (Figure S2D-G).

Meta-analysis of open-access FACS CRISPRi screen data identifies common and novel fluorescence modifiers

CRISPRBrain (https://crisprbrain.org/) contains many CRISPRi and CRISPRa screens on different cell types examining various phenotypes. We identified two FACS-based CRISPRi screens on iNeurons that identify modifiers of reactive oxygen species (CellRox) and lipid peroxidation (Liperfluo) using fluorescent indicators[11]. We performed an unbiased fixed effects meta-analysis of these two screens with our Halo-TDP-43 screen to determine if there were any common hits across screens. These common hits across multiple screens may be real hits that simultaneously downregulate TDP-43 and alter ROS-levels or lipid peroxidation; however, they may also be “false-positives” that are altering general proteostasis, general cellular stresses, or neuron-differentiation where phenotypes examined in these screens are a secondary or indirect effect of knockdown. Interestingly, comparison of z-scores between screens shows many genes that either positively or negatively regulate both our screen and the CRISPRBrain screens (Figure S3A-C). Indeed, graphing both meta-analyses together shows that most hits lie on a line with a slope of 1 ($r = 0.56$), indicating that these genes act similarly across screens with different modalities (Figure 3A). With the increased power from the multiple screens, we were able to identify novel hits that were underpowered previously (Figure 3A, S3A-C). Genes were considered “hits” if they were novel with directionality (either up or down) compared to the total population (the average of the hits in the CRISPRBrain screens. For the Halo-TDP-43 screens, genes were filtered by a LFC of 1 or -1 compared to the total population. We performed GO analysis on hits from the meta-analysis and found enrichment in many interesting categories, including ubiquitination, neddylation, autophagy, protein targeting, and cytoskeletal related terms (Figure 3B-E). On the other hand, some hits, like the BORC components, seem to be specific to our Halo-TDP-43 screen, so we chose to focus downstream analysis primarily on these hits that uniquely regulate TDP-43 biology. While this analysis provides a level of validation of our screen results, we picked genes from select categories to do a secondary, microscopy-based screen to further validate their effect on TDP-43 levels.

Validation of screen hits narrows in on BORC as a modifier of TDP-43 levels

We cloned single sgRNA plasmids for 59 genes that either increased or decreased Halo-TDP-43 in iNeurons but not in iPSCs. sgRNAs were transduced into iPSCs individually, followed by differentiation of iPSCs into iNeurons. We used automated microscopy and analysis to visualize and quantify the Halo-TDP-43 signal in cells after each gene knockdown (Figure 4A). 34 of 59 (58%) tested genes altered Halo-TDP-43 levels in the microscopy validation (Figure 4B-G, S4A-

D). For almost every gene, we observed an increase or decrease in Halo-TDP-43 levels without a change in Halo-TDP-43 localization or compartment specific level changes (Figure 4B). Since we used a single sgRNA plasmid for validation and not the dual guide plasmid used in the screen, some of the genes that did not pass this stage of validation may not have had sufficient gene knockdown in the validation to elicit the effect observed in the screen. However, we were interested primarily in the genes whose knockdown had the strongest effect on Halo-TDP-43 levels. To determine if results from Halo-TDP-43 expression assays also applied to endogenous, untagged TDP-43 levels, we selected 22 genes that passed Halo validation and performed immunofluorescence microscopy for endogenous (untagged) TDP-43 (Figure 4D-G, 5A-B, S4E-F). Of these, 18 (82%) gene knockdowns showed changes in endogenous TDP-43 levels (Figure 4D-G, S4E-F). However, many gene KDs, particularly genes involved in ubiquitination and m6A RNA methylation, changed untagged TDP-43 levels in the opposite direction as they change Halo-TDP-43 levels (Figure 4D-G). We posit that this Halo-untagged difference may be due to inherent destabilization of the HaloTagged TDP-43. KD of BORC subunit genes changed TDP-43 levels in the same direction for both Halo imaging and immunofluorescence (Figure 5A-B). To rule out the possibility of neighboring gene or off-target effects of CRISPRi, as has been reported previously[15], we examined the impact of BORC knockout (KO) on TDP-43 levels. Using the pLentiCRISPR system, which expresses the sgRNA of interest on the same plasmid as an active Cas9[16] we found that KO of BORCS7 using two different sgRNAs decreased TDP-43 levels by immunofluorescence (Figure 5C-D). Because of the known relationship between lysosomal dysfunction and FTD/ALS pathophysiology[17-23], we focused on the relationship between TDP-43 levels, lysosomal biology, and BORC.

Maintenance of neuronal TDP-43 requires active and neuritically localized lysosomes
As lysosomes are the primary recycling center of the cell, breaking down macromolecules into their subunits, we first asked whether lysosome activity was required to maintain TDP-43 levels. We treated Halo-TDP-43 neurons with various drugs that disrupt distinct processes in the lysosome pathway and asked if Halo-TDP-43 levels changed. Chloroquine (decreases lysosomal acidity), CTSBI (inhibits cathepsin B protease), ammonium chloride (NH_4Cl, inhibits lysosome-phagosome fusion), and GPN (ruptures lysosomal membranes) all consistently decreased Halo-TDP-43 levels (Figure 6A-B, S5A-C). The varied mechanisms of action of these drugs indicated that many lysosomal perturbations could alter TDP-43 levels. Further, two protein translation inhibitors, anisomycin and cycloheximide (CHX) also decreased Halo-TDP-43 levels (Figure 6A, S5B).

Having shown that functional lysosomes are required to maintain Halo-TDP-43 levels, we next tested the role of lysosome location in iNeurons. As the BORC complex is required for anterograde movement of lysosomes within axons of neurons[13, 24], we first asked whether Halo-TDP-43 is transported on lysosomes. Our previous work showed that mRNA transport granules can be transported on lysosomes and that overexpressed TDP-43 co-trafficked with lysosome-associated transport granules[25]. Indeed, in comparing motile Halo-TDP-43 with static Halo-TDP-43 in neurites, we found that motile TDP-43 was most often associated with lysosomes, not mitochondria (Figure 6C-D). Intriguingly, upon restricting lysosomes to the soma by knocking down a BORC subunit, we find that the fraction of motile Halo-TDP-43 in the periphery is reduced (Figure 6E, S5D).

TDP-43 mRNA levels are unchanged upon BORC KD
We next asked whether TDP-43 RNA levels were also changed. Using qPCR, we found TDP-43 mRNA levels were unchanged or slightly increased upon BORC KD. As expected, we observed

statistically significant reduction of TDP-43 mRNA upon TDP-43 KD via CRISPRi (Figure 7A, S6A). We then performed total RNA sequencing of BORCS6 KD iNeurons. While BORCS6 mRNA levels were reduced by ~50%, no change in TDP-43 mRNA levels occurred (Figure 7B-C), indicating that loss of BORC likely decreases TDP-43 protein levels independent of TDP-43 transcript expression.

As loss of BORC drastically changes the axonal transcriptome, particularly for mitochondrial genes[26], we wondered what the effect of BORC KD would be on the global transcriptome. We found that NT and BORC KD samples were substantially separated on a PCA plot, with over 90% of the variability between the samples being explained by a single principal component (Figure S6B). We found 98 upregulated genes and 139 downregulated genes (Figure 7D) in BORC KD neurons. GO analysis revealed an enrichment of terms related to neuron development and axon outgrowth (Figure 7E). As loss of TDP-43 can cause splicing changes and the inclusion of cryptic exons[27-29], we asked whether BORC KD decreased TDP-43 levels sufficiently to induce inclusion of cryptic exons[30, 31]. We did not observe an increase in expression of cryptic exons in genes that are commonly mis-spliced in iPSC-derived neurons after TDP-43 loss, including STMN2 and UNC13A. As such, BORC KD does not reduce TDP-43 protein levels sufficiently to cause functional loss of splicing repression.

TDP-43, like the proteome, shows longer turnover time in BORC KD neurons
As loss of BORC prevents the transport of lysosomes to axons[24, 26] and mRNAs can be transported on lysosomes to the periphery[25], we speculated that TDP-43 levels could be decreased in BORC KD iNeurons due to decreased axonal translation of TDP-43 mRNA. Using a TDP-43 mRNA N-terminally tagged with SunTag epitopes and with PP7 stem loops after the 3' UTR, we used microscopy to quantify the co-localization of TDP-43 new protein synthesis (SunTag signal) with mRNA (PP7-PCP signal)[32]. Surprisingly, we did not observe a change in TDP-43 translation (Figure S7A). As such, we hypothesized that loss of BORC might alter TDP-43 protein degradation rather than its synthesis. To test this hypothesis, we performed dynamic stable isotope labeling by amino acids in cell culture (dSILAC) to measure protein half-lives as well as whole neuron proteomics to measure protein abundances in BORCS6 KD and non-targeting iNeurons. We found that TDP-43 total protein levels are decreased in BORCS6 KD neurons (Figure 8A), further validating our earlier microscopy findings. We observed a similar trend for many proteins in the proteome (Figure 8B). Interestingly, TDP-43 shows longer half-life in BORCS6 KD neurons compared to the NT guide (Figure 8C), suggesting that protein degradation is potentially decreased in BORC KD iNeurons. We observed similar results for the total proteome, with many proteins showing longer turnover at day 7 in BORCS6 KD neurons compared to NT neurons (Figure 8D-E). Longer half-lives were also observed in d15 neurons although the changes in both abundance and half-life were reduced (Figure S7B-E), suggesting the neurons are better able to compensate for the loss of BORC at later time points. In comparing the KEGG and REACTOME terms shown as enriched in our proteins with longer turnover times in BORCS6 KD neurons (Figure 8F, S7F) to the mRNAs whose localization is altered in BORC KO neurons[26], we observe many of the same categories are enriched, including ribosome and biosynthetic pathways. As TDP-43 and the proteome show similar effects of BORCS6 KD on protein half-life, iNeurons are likely in steady state and making as much new heavy protein as they are degrading the light protein. As such, protein translation or protein degradation could be reduced. Although we did not observe a change in TDP-43 translation in our SunTag experiment, it may not be accurately reflecting the translation levels of TDP-43 due to the experimental necessity of over-expressing tagged TDP-43. As such, BORC may be affecting TDP-43 protein levels through a complicated mechanism.

Discussion

CRISPRi screens are powerful tools to identify novel pathways regulating cellular functions. Here, we use a CRISPRi FACS screen to identify the lysosome transport complex, BORC, as a modifier of TDP-43 protein, but not RNA, levels. A screen in iPSCs confirms that BORC specifically acts on TDP-43 in iNeurons. Additionally, we made use of publicly available CRISPRi screen data to perform a meta-analysis. This meta-analysis identified common pathways across screens, enabling us to focus on TDP-43-specific hits. Common pathway hits across screens involve genes related to ubiquitination, neddylation, and RNA modification. We think these pathways are related to generic protein level homeostasis in iPSC-derived neurons, and our findings suggest a general utility of meta-analysis of novel screens in the context of published screens to prioritize hits for follow-up and identify phenotype-specific pathways.

Knockout of individual BORC subunits impairs lysosomal transport, leading to lysosomal depletion in axons and altered transport of transcripts that hitchhike on lysosomes to the periphery[13, 24-26, 33, 34]. We initially hypothesized that loss of BORC would reduce neuritic translation of TDP-43. However, the lack of effect of BORC loss on TDP-43 mRNA or translation led us to focus on the role of lysosomes as a mechanism for how BORC affects TDP-43 protein levels. Surprisingly, we found that BORC loss leads to longer half-lives of TDP-43 and many other proteins. As lysosomes can be active in axons[35], this slower turnover may imply that lysosomes degrade proteins in axons and are important for maintaining axonal homeostasis locally. Perhaps restricting lysosomes to the soma leads to increased degradation of TDP-43 in the soma, altering the sensing of TDP-43 levels and careful homeostasis required to maintain those levels. Further work is needed to better understand this counterintuitive mechanism. TDP-43 protein levels are also altered by lysosome-inhibiting drug treatments, further demonstrating the requirement of active and properly localized lysosomes for maintenance of TDP-43 levels.

Defects in lysosome function and intracellular transport are associated with FTD/ALS[17, 36], but the evidence here that lysosomal mislocalization drives TDP-43 downregulation raises the possibility that this lysosomal dysfunction can be an upstream actor exacerbating TDP-43 loss of function phenotypes in disease. Interestingly, BORC KO in mice leads to neonatal death[33, 34] and mutations in BORCS8 cause an infantile neurodegeneration[37]. Importantly, anterograde TDP-43 transport and TDP-43 levels have not been interrogated in patients with this disorder, leading us to speculate that they have altered TDP-43 levels contributing to disease. As we were unable to detect cryptic exon formation in our BORC KD neurons, this potential TDP-43 loss of function in BORC patients may not lead to cryptic exon pathology observed in FTD/ALS patient tissue, so further work would be needed to understand the role of this intermediate TDP-43 loss in patients.

As TDP-43 pathology is associated with both loss and gain of function effects[6, 38, 39], understanding the pathways that lead to altered TDP-43 levels is crucial to identifying effective therapeutic targets for neurodegeneration. At the same time, the more specific these pathways are for TDP-43, the less likely treatments targeting these pathways will cause unwanted off-target effects. We demonstrate that CRISPRi screens are a powerful method to identify these specific pathways. Additionally, as more screens are performed and can be added to meta-analyses, we will gain further insight into non-specific pathways that affect protein levels and thus are unlikely to be effective therapeutic targets. In conclusion, these results provide important insight into the pathways affecting TDP-43 levels in neurons.

Methods

iPSC culture and neuron differentiation

Procurement and use of WTC11 cells from the Coriell cell repository followed all policies of the NIH Intramural research program. WTC11 cells were derived from an apparently healthy

30-year-old male. iPSC culture was performed following previously described protocols[40]. Briefly, iPSCs were grown in Essential 8 Medium (Thermo Fisher Scientific, A1517001) on tissue culture plates that had been coated with Matrigel (Corning, 354277). Medium was replaced daily or as needed. Accutase (Thermo Fisher Scientific, A1110501) was used to dissociate cells for passaging as single cells. 50 nM Chroman-1 (MedChemExpress, HY-15392) was added to promote survival after thaw and accutase treatment, until cell colonies had expanded to at least 4-5 cells/colony. The iPSCs used here were previously engineered to express mouse neurogenin-2 (mNGN2) with a doxycycline inducible promoter for neuronal differentiation (i11w-mN)[41]. Many experiments used a line that additionally expressed a catalytically inactive dCas9 fused to a KRAB transcriptional repression domain for CRISPRi knockdowns[10]. These engineered cells containing dCas9 are referred to here as i11w-mNC iPSCs.

iNeuron differentiation and culture was performed following previously described protocols[40]. Briefly, on day 0 of neuronal differentiation, iPSCs were passaged with accutase and plated on Matrigel-coated tissue culture plates. iPSCs were plated in induction media (knockout DMEM/F12 media (Life Technologies Corporation, #12660012) supplemented with N2 supplement (Life Technologies Corporation, 17502048), 1x GlutaMAX (Thermo Fisher Scientific, 35050061), 1x MEM nonessential amino acids (NEAA) (Thermo Fisher Scientific, 11140050), 50 nM Chroman-1, and 2 µg/mL doxycycline (Clontech, 631311)). Media was changed daily. On day 3 of neuronal differentiation, cells were passaged with accutase and plated on tissue culture plates that were coated with poly-L-ornithine (Sigma-Aldrich, P3655). Cells were plated in maturation media (BrainPhys media (Stemcell Technologies, 05790) supplemented with B27 Plus Supplement (Thermo Fisher Scientific, A3582801), 10 ng/mL BDNF (PeproTech, 450-02), 10 ng/mL NT-3 (PeproTech, 450-03), 1 µg/mL mouse laminin (Sigma, L2020-1MG), 50nM Chroman-1 (MedChem Express, HY-15392), and 2 µg/mL doxycycline (Clontech, 631311)). Half-media changes were performed every other day or every 3 days. Unless otherwise specified, all experiments were performed on day 7 neurons.

HaloTag knockin

1 million iPSCs were transfected with premixed 20 µg Alt-R™ A.s. Cas12a (Cpf1) V3 (IDT # 1081068), 200 pmol crRNA 5'-GGAAAAGTAAAAGATGTCTGAAT (IDT), and 10 µg knockin (KI) plasmid donor (gene-synthesized and cloned into pUC57 by Genscript; synthesized sequence contains HaloTag coding sequence inserted immediately downstream TDP-43 start codon ATG and flanked by 400 bp left and right homology arms) using Nucleofector 4D with buffer P3 and program CA-137 (Lonza) and then plated onto one well of rhLamin521 (Thermo) coated 6-well plate with StemFlex, RevitaCell (Thermo) and HDR enhancer V2 (IDT). Transfected cells were cultured in 32˚C incubator for 3 days before moving to 37˚C incubator, and fresh medium was changed daily after transfection. One week after transfection, the iPSCs were live stained with Oregon Green (Promega #G2801) following the manufacturer's protocol. Positive cells were sorted into 96-well Matrigel-coated plate at 1 cell/well with 100 µl/well StemFlex and 1x CloneR2 (Stem Cell Technologies). 10-12 days later, single-cell clones were picked and KI clones were confirmed by 5'-KI and 3'-KI junction genomic PCR (5KI-F: 5'-ATCGACTGGGACCTATCACG, 5KI-R: 5'-GCGTACCCTCGATAAAAACG; 3KI-F: 5'-GAGACCTTCCAGGCCTTCC, 3KI-R: 5'- TCTACAATCCCCAGTTTCCA). Heterozygous KI clones were further identified by the presence both non-KI and KI allele using primers recognizing homology arms (WT-F: 5'- GACGCATCATAAGCCTTCAG, WT-R: 5'-CCATGGATGAGACACACACC). Both non-KI and KI alleles were subject to Sanger sequencing to exclude heterozygous KI clones with indels in non-KI alleles.

Halo-TDP-43 CRISPRi FACS screen

Approximately 50 million Halo-TDP-43 iPSCs were transduced with a whole genome dual guide library[12] to a titer of approximately 70% in E8 with Chroman 1. The next day, the media was changed to E8 without chroman 1. The next day, iPSCs were split onto new Matrigel coated plates in E8 with chroman 1. The day following the split, iPSCs were treated with 8 µg/mL puromycin in E8 Chroman 1 to select for cells expressing an sgRNA. After selection, cells were split and differentiated into neurons following the standard protocol above. Some cells were maintained as iPSCs for the iPSC screen. On day 3 post dox induction, neurons were split onto final PLO-coated plates. On day 7 post dox induction, neurons were split for FACS. Papain solution (Worthington LK003176) was prepared by adding 20 mL TrypLE without phenol red (Gibco 12604-013) to one vial of papain and placing it at 37˚C for 10 minutes. Neurons were washed with PBS and then washed twice with PBS with 0.5 mM EDTA. Papain/TrypLE was added to neurons for 1-2 minutes at 37˚C. Papain was removed without disturbing the neuron sheet and trituration solution (Neuron culture media, 10 µM ROCK inhibitor, and one vial of DNAse freshly dissolved) was added to cells before transferring them to a conical tube. Cells were pipetted 3-10 times in the conical tube until cell clumps were gone. PBS was added to cells and cells were pelleted by centrifugation at 200 xg for 5 minutes. Neurons were resuspended in 1 mL Papain Inhibitor Media (27 mL trituration media with 3 mL Papain inhibitor) and incubated for 5-10 minutes. Cells were again pelleted by centrifugation at 200 xg for 5 minutes and resuspended in cell culture media before transferring cell suspension into a 5 mL collection 12x75 mm polypropylene FACS tube with 35-40 µm strainer cap. Cells were kept on ice until FACS was performed. Cells were sorted using the MoFlo Astrios cell sorter (Beckman Coulter), with Summit software (Beckman Coulter) to setup a sorting template. GFP positive cells were detected using the 488 nm laser excitation, and 520/30 nm filter for capturing signal emission. Halo was detected using 640 nm laser excitation and 675/30 nm filter for emission. The cells were first gated on GFP expression, which served as a highly expressing co-expression marker for sgRNA, and then gated on Halo expression, as follows. Four groups were collected from the FACS session: the bottom 25% of iPSCs expressing Halo-TDP-43, the top 25% of iPSCs expressing Halo-TDP-43, the bottom 25% of neurons expressing Halo-TDP-43, and the top 25% of neurons expressing Halo-TDP-43. Genomic DNA was collected from each fraction using the NucleoSpin Blood Kit (Macherey Nagel 740950.50) following manufacturer's instructions. Briefly, cells were washed in PBS and resuspended in PBS containing proteinase K. Next BQ1 was added to each tube and mixed by vortexing. Samples were incubated at 56˚C for 15 minutes and cooled to room temperature for at least 30 minutes. 100% ethanol was added to the tube and mixed by vortexing before loading onto the column. Columns were spun for 3 minutes at 4000 xg and flow through discarded. BQ2 was added to the column and columns spun for 2 minutes at 4000 xg. BQ2 step was repeated a total of 2 times. To elute genomic DNA, pre-heated BE was added to each column, incubated for 5 minutes at room temperature, and spun for 4 minutes at 4000 xg in a new tube. Elution was repeated a second time. Next, sgRNA amplicons were enriched using primers containing indexing barcodes and Illumina adapters. 10 µg of genomic DNA was used per PCR reaction. PCR reactions also contained 100 µM of one of the following indexed forward primer (caagcagaagacggcatacgagatcgctcagttctgctatgctgtttccagcttagctcttaaac, caagcagaagacggcatacgagattatctgaccttgctatgctgtttccagcttagctcttaaac, caagcagaagacggcatacgagatatatgagacgtgctatgctgtttccagcttagctcttaaac, caagcagaagacggcatacgagatcttatggaattgctatgctgtttccagcttagctcttaaac), 100 µM of one of the following indexed reverse primer (aatgatacggcgaccaccgagatctacactcgtggagcgagcacaaaaggaaactcaccctaactgt, aatgatacggcgaccaccgagatctacacctacaagataagcacaaaaggaaactcaccctaactgt, aatgatacggcgaccaccgagatctacactatagtagctagcacaaaaggaaactcaccctaactgt, aatgatacggcgaccaccgagatctacactgcctggtggagcacaaaaggaaactcaccctaactgt) and 1x NEBNext Ultra Q5 MasterMix (NEB M0544L). Cycling parameters were as follows: 98˚C for 30 seconds,

22-24 cycles of 98˚C for 10 seconds, 66˚C for 75 seconds, then a 5-minute hold at 72˚C after cycles and a hold at 4˚C. PCR reactions were pooled and leaned up with a PCR purification. A 0.5X-0.65X SPRI cleanup as performed prior to sequencing. Half volume of SPRI beads (Beckman Coulter B23318) were added to the pooled PCR reaction and incubated at room temperature for 10 minutes. Beads were removed with a magnet and supernatant collected. Next, a 0.65 volume of SPRI beads were added to cleared supernatant, incubated at room temperature for 10 minutes and tubes placed on a magnetic stand. Supernatant was removed and discarded. Beads were washed with fresh 80% ethanol twice and beads air dried for 2-5 minutes. Sample was eluted in 30 µL EB buffer. The SRPI PCR cleanup was repeated in its entirety to remove excess primer contamination. PCR product yield, size, and quality was checked on a Bioanalyzer (Agilent) with a High Sensitivity DNA chip (Agilent B23318). Enriched PCR product is 562 base pairs in length. Samples were sequenced on the MiSeq with 1% PhiX through paired end 50 sequencing with custom primers (Read1: gtgtgttttgagactataagtatcccttggagaaccaccttgttgg, Read2: tgctatgctgtttccagcttagctcttaaac, i7 Indexing primer: aagagctaagctggaaacagcatagca). Sequencing files were demultiplexed based on the sample PCR. To remove recombined dual guides, fastq files were filtered for reads containing paired guides for the same target gene using the parser.py file (https://github.com/NIH-CARD). The parsed dual hits file was analyzed using the standard MAGeCKFlute robust ranked algorithm (RRA) pipeline[42] comparing the high 25% to low 25% of the TDP-43 HaloTag fluorescence. The RRA uses a negative binomial model to generate p-values to rank guides from negative to positive. Guide output files were filtered to remove low count guides and used to generate rank plots of target guides and non-targeting negative controls. All data and code for plots is available on (https://github.com/jhawrot/TDP_BORC/tree/main).

CRISPRi meta-analysis

CRISPRi FACS screens in i^{3}Neurons[11] were obtained from CRISPRBrain (https://crisprbrain.org/) and the Kampmann lab and underwent data harmonization with the screens presented here. First, screen phenotype scores and log fold changes were aligned by converting effect estimates to standardized beta values represented by z-scores. Next, extreme p-values were stabilized by truncation to prevent distortions in the statistical tests due to outliers or very small probabilities, ensuring a robust meta-analysis, accommodating the floating point of the system and acknowledging that this truncation will cause results to be more conservative. Standard errors of the effect estimates were derived by dividing the beta estimate by the absolute value of the z-scores. Fixed effect meta-analyses were then carried out for all possible screen combinations (combining already published versus novel screens). These functions calculate pooled estimates of effect sizes, variance, and test for heterogeneity among screens. Novelty was assessed by filtering associations that were not significant after multiple test corrections in either of the constituent datasets but were significant after false-discovery rate adjustment of the meta-analysis. Data was visualized using modified MAGeCKFlute pipelines to assess putative biological functions of significant genes using published enrichment functions including clusterProfiler, GOstats, enrich.HGT, and GSEA packages. TDP-43 expression hits were grouped into positive and negative modifiers using Log2FC values, and statistical significance was assessed by gene ratio or FDR depending on the enrichment analysis. Code is available on (https://github.com/NIH-CARD).

Lentivirus production and transduction

Individual CRISPRi knockdowns were performed by cloning sgRNAs into pU6-sgRNA EF1Alpha-puro-T2A-BFP (Addgene plasmid # 60955). sgRNA sequences for screen validation are listed in Table S1. To make lentivirus, Lenti-X human embryonic kidney (HEK) cells were split with trypsin, plated on poly-L-ornithine coated plates, and allowed to recover. Cells were

then transfected with sgRNA plasmids on a 6 well plate using 3.75 µL Lipofectamine 3000 Reagent and 5 µL P3000 Enhancer Reagent (Invitrogen, L3000075), Opti-MEM (Gibco, 31985062), psPAX2 F46, pMD2G F45, and pAdVantage F44. Transfected cells were cultured for two days in DMEM supplemented with GlutaMAX--I (Thermo Fisher Scientific, 35050061) and 10% Fetal Bovine Serum (FBS) (Sigma-Aldrich, F4135). Media was then changed and supplemented with (1:500) viral boost reagent (ALSTEM, VB100), and cells were cultured for two days before media was harvested and Lenti-X Concentrator (Takara Bio USA, 631231) was added at (1:3) to concentrate the virus for 2-3 days at 4°C. Virus was then collected, aliquoted, and stored at -80°C until use.

iPSCs were transduced at scales of 0.1-1e6 cells per 100 µL concentrated virus while cells were in suspension. Cells were allowed to recover for two days before 10 µg/mL puromycin dihydrochloride (Sigma-Aldrich, P9620) was added for selection. For cells that were differentiated, transduction was performed four days before initiating neuronal differentiation.

Validation of hits from genome wide screens

Hits from the screen were validated by microscopy with individual sgRNA knockdowns in i11w-hT neurons. Cells were plated, transduced, and differentiated as described above. Fluorescent HaloTag ligand JF646 (Promega, GA112A) was added at 200 µg/mL approximately 15 minutes before microscopy. Cells were imaged on Nikon Ti2 with automated stage at 20x with exposure times of 100ms for all channels. Laser power was as follows: 640 nm at 100%, 405 nm at 25%, and 561 nm at 100%. Halo-TDP-43 fluorescent intensity was quantified using CellProfiler[43] or Nikon Elements General Analysis 3 and graphed in GraphPad Prism.

sgRNAs for genes selected for further validation on untagged TDP-43 were transduced into i11w-mNC iPSCs and neurons differentiated as above. On day 7, neurons were fixed with 4% PFA (Thermo Fisher Scientific, 28906) for 10 minutes at room temperature. PFA was removed and cells washed in PBS. Cells were then permeabilized with 0.1% Triton-X 100 (Sigma-Aldrich, 93443) for 10 minutes before blocking in 2% bovine serum albumin (BSA) (Jackson ImmunoResearch, 001-000-162) for 10 minutes. TDP-43 primary antibody (Proteintech, 10782-2-AP) was diluted 1:1000 in 2% BSA and added to cells at 4˚C overnight. After washing, Donkey Anti-Rabbit IgG (H+L), Highly Cross-Adsorbed secondary antibody (CF488, Biotium, 20015) was added at 1:1000 in 2% BSA for 1 hour at room temperature. Cells were washed and DRAQ5 nuclear stain (Thermo Fisher Scientific, 62251) was added at 1:1000 dilution in PBS for 5 minutes. DRAQ5 was washed out with PBS three times before imaging. Stained cells were imaged on Nikon Ti2 with automated stage at 20x and an exposure time of 100 ms for 640nm and 488nm and 200 ms for 405nm. Laser power was 100% for all channels. TDP-43 fluoresce intensity was quantified using Nikon Elements and graphed in GraphPad Prism.

Lysosome drug treatment

i11w-hT iPSCs were cultured and differentiated into neurons. i11w-mNC, treated for 24 hours with DMSO, were used as a Halo-negative control. Microscopy was performed on day 7 of neuronal differentiation. Wells were individually treated with drugs by removing half the media and adding back an equal volume of media containing 2x final concentration of each drug, for timepoints as stated below. A volume of DMSO equal to the largest volume of drug was added at the earliest timepoint to wells as a negative control for treatment. Treatments were as follows: 50 µM Chloroquine (Selleck Chemicals, S6999) for 24 hours; 50 µM CA-074me (Selleck Chemicals, S6999), a Cathepsin B Inhibitor (CTSBI), for 6 hours; 30 mM Ammonium Chloride (NH_4Cl) (Sigma-Aldrich, A9434) for 5 hours; 500 nM Bafilomycin A1 (BafA1) (LKT Labs, B0025) for 4 hours; 1x Lysosome Protease Inhibitor Cocktail (20 µM E64 (Selleck Chemicals, S7379),

10 μM pepstatin A (Selleck Chemicals, S7381) and 50 μM leupeptin (Sigma-Aldrich, L2884); referred to in Figure S5B-C as Protease Inhibitor) for 4 hours; 1 mM L-Leucyl-L-Leucine methyl ester (hydrochloride) (LLOME) (Cayman Chemical Company, 16008) for 4 hours; 400 μM Gly-Phe-β-naphthylamide (GPN) (Cayman Chemical Company, 14634) for 1 hour; 500 μM Sodium (meta) arsenite (NaAsO2) (Sigma-Aldrich, S7400), 1 hours; 40 μM Anisomycin (Sigma-Aldrich, A5862) for 1 hour; and 0.1 mg/mL Cycloheximide solution (CHX) (Sigma-Aldrich, C4859) for 45 minutes. Fluorescent HaloTag ligand was added as described above 15 minutes prior to imaging. Cells were imaged on Nikon Ti2 with automated stage at 20x in 640nm with an exposure time of 100ms and 100% laser power. Halo-TDP-43 fluorescent intensity was quantified using Nikon Elements and graphed in GraphPad Prism.

Live cell imaging of TDP-43 motion and organelle co-localization

i11w-hT iPSCs were transduced with fluorescent tags for mitochondrial targeted mEmerald and LAMP1 tagged with mApple. The cells were then transduced with either BORCS6 or BORCS7 knockdown and non-targeting control guides. BORCS6 knockdown cells were cultured and differentiated as described above. BORCS7 knockdown cells were differentiated as neurospheres. Fluorescent HaloTag ligand was added to day 7 BORCS6 knockdown neurons and day 10 BORCS7 knockdown neurospheres, as described above. Cells were imaged on Nikon Ti2 with automated stage at 60x and exposure times of 100 ms for all channels. Laser power was 100% for 640nm and 561nm. 405nm and 488nm lasers were set at 100% and 99.4%, respectively, for BORCS6 knockdown cells, and at 50% for BORCS7 knockdown neurospheres. DAPI image was taken once at the beginning of the video; GFP, Cy5, and RFP channels were captured over 30 seconds with no delay between frames and an approximate frames per second (FPS) of 1.16. Puncta were counted from kymographs of axonal segments made in ImageJ or Nikon Elements and graphed in GraphPad Prism.

qPCR

qPCR was performed using TaqMan Real-Time PCR assays. RNA was extracted from BORC and TDP-43 knockdown and non-targeting control i11-mNC-derived neurons using the RNeasy Plus Mini kit (QIAGEN, 74134). RNA concentrations were measured with a DeNovix DS-11 FX+ 1uL Spectrophotometer, and 855 ng of RNA was used as input for reverse transcription. Reverse transcription was performed using the High-Capacity cDNA Reverse Transcription Kit (Thermo Fisher Scientific, 4368814). The qPCR reaction was performed with 2x TaqMan Universal PCR Master Mix (Thermo Fisher Scientific, 4304437) on an Applied Biosystems QuantStudio 6 Flex Real-Time PCR System. Probes were run singleplex. The Taqman probe for the target was TARDBP, (FAM-MGB Hs00606522_m1, Thermo Fisher Scientific, 4453320). Two endogenous controls were used: PPIA (VIC-MGB-PL Hs04194521_s1, Thermo Fisher Scientific, 4448484); and PGK1, TaqMan ID: Hs00943178_g1, VIC-MGB-PL, (Thermo Fisher Scientific, 4448484). Relative change in gene expression was examined using the 2^-(ΔΔCt) analysis method[44]. Significance was evaluated using an ordinary one-way ANOVA with the Šidák correction for multiple comparisons.

pLentiCRISPR

A non-targeting (AGAGTTACGTCGCTTCGATC) and two sgRNA targeting sequences against BORCS7 (1: CGCGATTACGTCAGTACCAC, 2: GATTACGTCAGTACCACAGG) were cloned into the lenti-CRISPR v2 plasmid (Addgene 52961) following the Zhang Lab protocol (https://media.addgene.org/data/plasmids/52/52961/52961-attachment_B3xTwla0bkYD.pdf). Briefly, the plasmid was digested with BsmBI-v2 (NEB R0739), the cut vector was dephosphorylated with NEB Quick CIP (NEB M0525), and digested and dephosphorylated vector was extracted from an agarose gel. Primers containing the sgRNA targeting sequences

(Eurofins) were phosphorylated with T4 PNK (NEB M0201) and annealed before being ligated into the cut vector using 2x Ligation Master Mix (Takara 6023). After sequencing to confirm correct cloning, plasmids were transfected into Lenti-X HEK cells using standard protocols (see above). Virus was then transduced into i11w-mN iPSCs and selected with puromycin using standard protocols (see above). Selected iPSCs were differentiated using standard protocols (see above). On day 7 post dox induction, neurons were fixed and immunofluorescence performed as above.

SunTag TDP-43 translation assay

TDP-43 coding sequence and 3'UTR were cloned into a plasmid expressing 24 SunTag repeats under an Ef1alpha promoter followed by 24 PP7 stem loops[32] (modified from Addgene 74928). This plasmid was transfected into iPSCs stably expressing the SunTag scFv tagged with HaloTag under an Ef1alpha promoter (modified from Addgene 60907), PP7 coat protein tagged to 3 SnapTags (synthesized), and mEmerald-tagged lysosomes (to validate BORC KD). iPSCs were transduced with sgRNA and differentiated as spheres before plating on an 8 well glass bottom µ-Slide (Ibidi, 80827). Neurospheres were imaged at d10 post dox induction on a Nikon Ti2 spinning disk confocal microscope at 60x with only neurites in the field of view. Exposure times were as follows: 300 ms for 640nm, 200 ms for 561, 200 ms for 488, and 100ms for 405. Laser power was at 50% for DAPI and 100% for all other channels. Images were quantified for co-localized PP7 and SunTag (SnapTag and HaloTag, respectively) puncta using Nikon Elements. Resulting data were graphed in GraphPad Prism.

RNA sequencing

RNA was extracted from day 7 BORCS6 knockdown and non-targeting control i11-mNC neurons using the Direct-zol-96 MagBead RNA kit (Zymo Research, R2103). Manufacturer protocol was followed, including the optional DNAase step, with volumes increased for an automated run on the KingFisher. Quantified with Qbit and frozen at -80°C. RNA quality was checked on a BioAnalyzer and Strand-Specific RNA-seq library preparation was performed with rRNA depletion using the NEBNext® Ultra™ II Directional RNA Library Prep Kit for Illumina® (New England Biolabs, E7760) and the NEBNext® Globin & rRNA Depletion Kit. (New England Biolabs, E7750). Samples were run on an Illumina NovaSeq X 10B on a 2 x 150 bp flow cell.

Bulk RNA sequencing analysis

Gene length normalized counts per gene were generated and then within sample normalization using counts per million (cpm) was performed. Next, pedestalling using a value of 2 and log2 transformation were performed. Cyclicloess was used to normalize expression across samples followed by exploratory analysis to insepct for and remove outlier samples if present. If present, cyclicloess nomrlaization is repeated. Data post cyclicloess normalization is then noise modeled (CV~mean) by experiment condition (NT v KD) and a noise threshold for the data defined. This noise threshold is then used to filter remove noise-biased genes with surviving genes then subject to differential testing using the appropriate test. After differential testing, all statistics are captured and exported along with confirmatory visual generation post differential gene selection. Pathway analysis was performed to identify enriched pathways and functions for each comparison performed as part of differential testing.

Cryptic splicing analysis

For cryptic splicing analyses, sequencing files were aligned to GRCh38 reference genome (STAR v2.7.3a)[45]. We ran MAJIQ (v2.1)[46] on aligned BAM files using a custom Snakemake (v 5.5.4)[47] pipeline (https://github.com/frattalab/splicing). A threshold of 10% difference in percent spliced in (PSI, ΔΨ) was used to identify a significant change between groups. We defined cryptic splicing as junctions with ΔΨ > 10% that were present in <5% of

control samples or ΔΨ < -10% that were present in >10% of control samples. An additional pipeline developed previously[31] was used to visualize and categorize each mis-spliced junction as cryptic exon, exon skipping, intron retention, or canonical junction (https://github.com/NIH-CARD/proteogenomic-pipeline).

Proteomic sample preparation

BORC knockdown and non-targeting control i11w-mNC cells were cultured and differentiated as described above until day 5 of neuronal differentiation. On day 5, half of the cultures were changed to heavy-SILAC media ("dSILAC samples"), which was DMEM for SILAC (Thermo Fisher Scientific, 88364) supplemented with B27 Plus Supplement (Thermo Fisher Scientific, A3582801), 10 ng/mL BDNF (PeproTech, 450-02), 10 ng/mL NT-3 (PeproTech, 450-03), 1 µg/mL mouse laminin (Sigma, L2020-1MG), 50 nM Chroman-1 (MedChemExpress Catalog #HY-15392), 2 µg/mL doxycycline (Clontech, 631311), 0.5 mM lysine, and 0.3 mM arginine. Heavy SILAC media was supplemented with L-Lysine:2HCl (13C6, 99%; 15N2, 99%) (Cambridge Isotope Laboratories, Inc., CNLM-291-H) and L-Arginine:HCl (13C6, 99%; 15N4, 99%) (Cambridge Isotope Laboratories, Inc., CNLM-539-H). Remaining cultures were maintained in light SILAC media made with L-Lysine monohydrochloride (SIGMA, L8662 and L7039) and L-Arginine monohydrochloride (SIGMA, A4599) to produce non-SILAC samples to evaluate changes in total protein abundance. Half-media changes were performed every other day or every 3 days. Cells were harvested on day 7 and day 15 post-dox induction.

Protein was extracted from day 7 and day 15 neurons for mass spectrometry as done previously[48]. Neurons were gently washed with PBS, then SP3 lysis buffer (50 mM Tris-HCl (Thermo Fisher Scientific, 15568025), 50 mM NaCl (Thermo Fisher Scientific, 24740011), 1% SDS (Thermo Fisher Scientific, 15553027), 1% Triton X-100 (MilliporeSigma, X100), 1% NP-40 (Thermo Fisher Scientific, 85124), 1% Tween 20 (MilliporeSigma, P9416), 1% glycerol (MP Biomedicals, 800687), 1% Sodium deoxycholate (wt/vol) (MilliporeSigma D6750), 5 mM EDTA, 5mM Dithiothreitol (DTT) (Thermo Fisher Scientific, R0862), 5 KU Benzonase (Sigma-Aldrich, E8263), and 1× cOmplete ULTRA Protease Inhibitor Tablets (one tablet per 10mL of lysis buffer) (Sigma-Aldrich, 5892791001)) was added directly to the wells. Neurons were scraped into the buffer to aid with lysis. Proteins were alkylated with 10 mM Iodoacetamide (IAA) (Thermo FIsher Scientific, A39271) at room temperature in the dark, then reduced by adding 2 µL of 500 mM DTT to the lysate and incubating at 25˚C for 30 min in the light. A Thermo Fisher KingFisher Apex was used to perform the automated SP3 protein enrichment protocol. This protocol uses SP3 beads: GE SpeedBeads (GE45152105050250) and of GE SpeedBeads (GE65152105050250) combined in a 1:1 ratio. The SP3 beads are washed in LC-MS grade water (Pierce, 51140) and reconstituted in 50% EtOH at a concentration of 4 mg/mL. Samples are diluted 1:1 with 100% EtOH, washed in 80% EtOH, and eluted in 50 mM ammonium bicarbonate with 20 µg/mL lyophilized trypsin/LysC (Promega, V5073). After completion of the KingFisher SP3 protocol, samples were shaken overnight at 37˚C. The KingFisher was used to perform a bead removal protocol twice. Solvents were removed in a speed vac. Samples were stored dry at -20˚C until resuspension in 2% acetonitrile (Thermo Fisher Scientific, 51101), 0.4% Trifluoroacetic acid (TFA) (Thermo Fisher Scientific, 85183), and 0.1% formic acid (Thermo Fisher Scientific, 28905).

LC-MS analysis

Peptide concentration from each sample was measured on a DeNovix DS-11 FX+ 1uL Spectrophotometer and normalized to 0.5 µg/µL. LC-MS/MS experiments were performed on a Thermo Scientific Orbitrap Lumos Tribrid Mass Spectrometer couple with a Thermo Scientific Ultimate 3000 HPLC system. The injection volume for each sample was 2 µl. Peptides were

separated on a Thermo Scientific ES902 column (particle Size: 2 µm, diameter: 75 µm, length: 25 cm). Mobile phase A contains 0.1% formic acid in LC-MS grade water, and Mobile phase B contains 0.1% formic acid in LC-MS grade acetonitrile. Mobile phase B was increased from 3% to 22% in 64 min, then from 22% to 36% in 8 min. LC-MS/MS data were acquired in data-dependent mode. The MS1 scans were performed in orbitrap with a resolution of 120K, a mass range of 375-1500 m/z, and an AGC target of 4 x 105. The quadrupole isolation window is 1.6 m/z. The precursor ion intensity threshold to trigger the MS/MS scan was set at 1 x 104. MS2 scans were conducted in the ion trap. Peptides were fragmented with the HCD method and the collision energy was set at 30%. The maximum ion injection time was 35 ms. MS1 scan was performed every 3 sec. As many MS2 scans were acquired within the 3-sec cycle.

Proteomic data analysis

Proteomic raw data were analyzed using MaxQuant software (v. 1.6.14)[49]. A reviewed Swiss-Prot *Homo sapiens* database and a custom neuron-specific contaminant FASTA library[50] (available to download at https://github.com/HaoGroup-ProtContLib) were used for protein and peptide identifications with a 1% false discovery rate cutoff. A maximum of two missed cleavages were allowed. A maximum of three variable modifications were allowed for cysteine N-ethylmaleimide, methionine oxidation, and protein N-terminus acetylation. Precursor and fragment tolerances were set to 25 ppm. Contaminatn proteins and peptides were removed. Protein intensities from protein.txt output files were used for nonSILAC data analysis. dSILAC data was analyzed using a previously established workflow[51]. A standard multiplicity with two labels was enabled for SILAC data, and Lys8/Arg10 was selected as the heavy channel. For SILAC proteomics, only y-type product ions with up to two charges were used for quantification. The "peptide.txt" report was exported for subsequent analysis in R. Peptides from contaminant proteins and peptides with intensities below 1000 were removed. Peptides with heavy/light ratios lower than 0.01 or higher than 100 were also removed to avoid outlier half-life measurements. A single timepoint calculation was used to calculate peptide half-lives assuming a steady state of turnover: $t_{1/2} = t_s \times \frac{ln\,(2)}{ln\,(1+R)}$, where R is the heavy-to-light ratio and ts is the labeling time point after media switch as described previously[51]. Protein half-lives were then determined as the harmonic mean of half-lives from unique peptides belonging to each protein.

Acknowledgements

We thank Sami Barmada, Derek Narendra, and Achim Werner for their insights into the best genes from the screens to follow up on within their subject matter expertise. We thank the NIH Intramural Sequencing Center for performing RNA sequencing, the Sequencing Cores at the National Heart, Lung, and Blood Institute for sequencing screen samples, and the Proteomics Core at the National Institute of Neurological Disorders and Stroke for performing mass spec. This work was supported by the National Institute of Neurological Disorders and Stroke and the Center for Alzheimer's and Related Dementias, within the Intramural Research Program of the National Institute on Aging, National Institutes of Health, Department of Health and Human Services. M.E.W. was additionally supported by funding through the Chan Zuckerberg Initiative. V.H.R. was supported in part by the National Institute of General Medical Sciences Fi2GM142475. L.H. was supported in part by the National Institute of Neurological Disorders and Stroke R01NS121608.

References

1. Meneses A, Koga S, O'Leary J, Dickson DW, Bu G, Zhao N. TDP-43 Pathology in Alzheimer's Disease. Mol Neurodegener. 2021;16(1):84. Epub 20211220. doi: 10.1186/s13024-021-00503-x. PubMed PMID: 34930382; PMCID: PMC8691026.

2. Tziortzouda P, Van Den Bosch L, Hirth F. Triad of TDP43 control in neurodegeneration: autoregulation, localization and aggregation. Nat Rev Neurosci. 2021;22(4):197-208. Epub 20210302. doi: 10.1038/s41583-021-00431-1. PubMed PMID: 33654312.
3. Baughn MW, Melamed Z, Lopez-Erauskin J, Beccari MS, Ling K, Zuberi A, Presa M, Gonzalo-Gil E, Maimon R, Vazquez-Sanchez S, Chaturvedi S, Bravo-Hernandez M, Taupin V, Moore S, Artates JW, Acks E, Ndayambaje IS, Agra de Almeida Quadros AR, Jafar-Nejad P, Rigo F, Bennett CF, Lutz C, Lagier-Tourenne C, Cleveland DW. Mechanism of STMN2 cryptic splice-polyadenylation and its correction for TDP-43 proteinopathies. Science. 2023;379(6637):1140-9. Epub 20230316. doi: 10.1126/science.abq5622. PubMed PMID: 36927019; PMCID: PMC10148063.
4. Arnold ES, Ling SC, Huelga SC, Lagier-Tourenne C, Polymenidou M, Ditsworth D, Kordasiewicz HB, McAlonis-Downes M, Platoshyn O, Parone PA, Da Cruz S, Clutario KM, Swing D, Tessarollo L, Marsala M, Shaw CE, Yeo GW, Cleveland DW. ALS-linked TDP-43 mutations produce aberrant RNA splicing and adult-onset motor neuron disease without aggregation or loss of nuclear TDP-43. Proc Natl Acad Sci U S A. 2013;110(8):E736-45. Epub 20130204. doi: 10.1073/pnas.1222809110. PubMed PMID: 23382207; PMCID: PMC3581922.
5. Highley JR, Kirby J, Jansweijer JA, Webb PS, Hewamadduma CA, Heath PR, Higginbottom A, Raman R, Ferraiuolo L, Cooper-Knock J, McDermott CJ, Wharton SB, Shaw PJ, Ince PG. Loss of nuclear TDP-43 in amyotrophic lateral sclerosis (ALS) causes altered expression of splicing machinery and widespread dysregulation of RNA splicing in motor neurones. Neuropathol Appl Neurobiol. 2014;40(6):670-85. doi: 10.1111/nan.12148. PubMed PMID: 24750229.
6. Ling SC, Polymenidou M, Cleveland DW. Converging mechanisms in ALS and FTD: disrupted RNA and protein homeostasis. Neuron. 2013;79(3):416-38. doi: 10.1016/j.neuron.2013.07.033. PubMed PMID: 23931993; PMCID: PMC4411085.
7. Mackenzie IR, Neumann M. Reappraisal of TDP-43 pathology in FTLD-U subtypes. Acta Neuropathol. 2017;134(1):79-96. Epub 20170502. doi: 10.1007/s00401-017-1716-8. PubMed PMID: 28466142.
8. Nana AL, Sidhu M, Gaus SE, Hwang JL, Li L, Park Y, Kim EJ, Pasquini L, Allen IE, Rankin KP, Toller G, Kramer JH, Geschwind DH, Coppola G, Huang EJ, Grinberg LT, Miller BL, Seeley WW. Neurons selectively targeted in frontotemporal dementia reveal early stage TDP-43 pathobiology. Acta Neuropathol. 2019;137(1):27-46. Epub 20181203. doi: 10.1007/s00401-018-1942-8. PubMed PMID: 30511086; PMCID: PMC6339592.
9. Doench JG. Am I ready for CRISPR? A user's guide to genetic screens. Nat Rev Genet. 2018;19(2):67-80. Epub 20171204. doi: 10.1038/nrg.2017.97. PubMed PMID: 29199283.
10. Tian R, Gachechiladze MA, Ludwig CH, Laurie MT, Hong JY, Nathaniel D, Prabhu AV, Fernandopulle MS, Patel R, Abshari M, Ward ME, Kampmann M. CRISPR Interference-Based Platform for Multimodal Genetic Screens in Human iPSC-Derived Neurons. Neuron. 2019;104(2):239-55 e12. Epub 20190815. doi: 10.1016/j.neuron.2019.07.014. PubMed PMID: 31422865; PMCID: PMC6813890.
11. Tian R, Abarientos A, Hong J, Hashemi SH, Yan R, Drager N, Leng K, Nalls MA, Singleton AB, Xu K, Faghri F, Kampmann M. Genome-wide CRISPRi/a screens in human neurons link lysosomal failure to ferroptosis. Nat Neurosci. 2021;24(7):1020-34. Epub 20210524. doi: 10.1038/s41593-021-00862-0. PubMed PMID: 34031600; PMCID: PMC8254803.
12. Replogle JM, Bonnar JL, Pogson AN, Liem CR, Maier NK, Ding Y, Russell BJ, Wang X, Leng K, Guna A, Norman TM, Pak RA, Ramos DM, Ward ME, Gilbert LA, Kampmann M, Weissman JS, Jost M. Maximizing CRISPRi efficacy and accessibility with dual-sgRNA libraries and optimal effectors. Elife. 2022;11. Epub 20221228. doi: 10.7554/eLife.81856. PubMed PMID: 36576240; PMCID: PMC9829409.

13. Pu J, Schindler C, Jia R, Jarnik M, Backlund P, Bonifacino JS. BORC, a multisubunit complex that regulates lysosome positioning. Dev Cell. 2015;33(2):176-88. doi: 10.1016/j.devcel.2015.02.011. PubMed PMID: 25898167; PMCID: PMC4788105.
14. Avendano-Vazquez SE, Dhir A, Bembich S, Buratti E, Proudfoot N, Baralle FE. Autoregulation of TDP-43 mRNA levels involves interplay between transcription, splicing, and alternative polyA site selection. Genes Dev. 2012;26(15):1679-84. doi: 10.1101/gad.194829.112. PubMed PMID: 22855830; PMCID: PMC3418585.
15. Replogle JM, Saunders RA, Pogson AN, Hussmann JA, Lenail A, Guna A, Mascibroda L, Wagner EJ, Adelman K, Lithwick-Yanai G, Iremadze N, Oberstrass F, Lipson D, Bonnar JL, Jost M, Norman TM, Weissman JS. Mapping information-rich genotype-phenotype landscapes with genome-scale Perturb-seq. Cell. 2022;185(14):2559-75 e28. Epub 20220609. doi: 10.1016/j.cell.2022.05.013. PubMed PMID: 35688146; PMCID: PMC9380471.
16. Sanjana NE, Shalem O, Zhang F. Improved vectors and genome-wide libraries for CRISPR screening. Nat Methods. 2014;11(8):783-4. doi: 10.1038/nmeth.3047. PubMed PMID: 25075903; PMCID: PMC4486245.
17. Root J, Merino P, Nuckols A, Johnson M, Kukar T. Lysosome dysfunction as a cause of neurodegenerative diseases: Lessons from frontotemporal dementia and amyotrophic lateral sclerosis. Neurobiol Dis. 2021;154:105360. Epub 20210331. doi: 10.1016/j.nbd.2021.105360. PubMed PMID: 33812000; PMCID: PMC8113138.
18. Rhinn H, Tatton N, McCaughey S, Kurnellas M, Rosenthal A. Progranulin as a therapeutic target in neurodegenerative diseases. Trends Pharmacol Sci. 2022;43(8):641-52. Epub 20220115. doi: 10.1016/j.tips.2021.11.015. PubMed PMID: 35039149.
19. Hung C, Patani R. 4R tau drives endolysosomal and autophagy dysfunction in frontotemporal dementia. Autophagy. 2024;20(5):1201-2. Epub 20240109. doi: 10.1080/15548627.2023.2300917. PubMed PMID: 38174587; PMCID: PMC11135858.
20. Wallings RL, Humble SW, Ward ME, Wade-Martins R. Lysosomal Dysfunction at the Centre of Parkinson's Disease and Frontotemporal Dementia/Amyotrophic Lateral Sclerosis. Trends Neurosci. 2019;42(12):899-912. Epub 20191105. doi: 10.1016/j.tins.2019.10.002. PubMed PMID: 31704179; PMCID: PMC6931156.
21. Talaia G, Bentley-DeSousa A, Ferguson SM. Lysosomal TBK1 responds to amino acid availability to relieve Rab7-dependent mTORC1 inhibition. EMBO J. 2024. Epub 20240805. doi: 10.1038/s44318-024-00180-8. PubMed PMID: 39103493.
22. Ling SC, Dastidar SG, Tokunaga S, Ho WY, Lim K, Ilieva H, Parone PA, Tyan SH, Tse TM, Chang JC, Platoshyn O, Bui NB, Bui A, Vetto A, Sun S, McAlonis-Downes M, Han JS, Swing D, Kapeli K, Yeo GW, Tessarollo L, Marsala M, Shaw CE, Tucker-Kellogg G, La Spada AR, Lagier-Tourenne C, Da Cruz S, Cleveland DW. Overriding FUS autoregulation in mice triggers gain-of-toxic dysfunctions in RNA metabolism and autophagy-lysosome axis. Elife. 2019;8. Epub 20190212. doi: 10.7554/eLife.40811. PubMed PMID: 30747709; PMCID: PMC6389288.
23. Beckers J, Tharkeshwar AK, Van Damme P. C9orf72 ALS-FTD: recent evidence for dysregulation of the autophagy-lysosome pathway at multiple levels. Autophagy. 2021;17(11):3306-22. Epub 20210226. doi: 10.1080/15548627.2021.1872189. PubMed PMID: 33632058; PMCID: PMC8632097.
24. Farias GG, Guardia CM, De Pace R, Britt DJ, Bonifacino JS. BORC/kinesin-1 ensemble drives polarized transport of lysosomes into the axon. Proc Natl Acad Sci U S A. 2017;114(14):E2955-E64. Epub 20170320. doi: 10.1073/pnas.1616363114. PubMed PMID: 28320970; PMCID: PMC5389300.
25. Liao YC, Fernandopulle MS, Wang G, Choi H, Hao L, Drerup CM, Patel R, Qamar S, Nixon-Abell J, Shen Y, Meadows W, Vendruscolo M, Knowles TPJ, Nelson M, Czekalska MA, Musteikyte G, Gachechiladze MA, Stephens CA, Pasolli HA, Forrest LR, St George-Hyslop P, Lippincott-Schwartz J, Ward ME. RNA Granules Hitchhike on Lysosomes for Long-Distance

Transport, Using Annexin A11 as a Molecular Tether. Cell. 2019;179(1):147-64 e20. doi: 10.1016/j.cell.2019.08.050. PubMed PMID: 31539493; PMCID: PMC6890474.
26. De Pace R, Ghosh S, Ryan VH, Sohn M, Jarnik M, Rezvan Sangsari P, Morgan NY, Dale RK, Ward ME, Bonifacino JS. Messenger RNA transport on lysosomal vesicles maintains axonal mitochondrial homeostasis and prevents axonal degeneration. Nat Neurosci. 2024;27(6):1087-102. Epub 20240410. doi: 10.1038/s41593-024-01619-1. PubMed PMID: 38600167; PMCID: PMC11156585.
27. Mehta PR, Brown AL, Ward ME, Fratta P. The era of cryptic exons: implications for ALS-FTD. Mol Neurodegener. 2023;18(1):16. Epub 20230315. doi: 10.1186/s13024-023-00608-5. PubMed PMID: 36922834; PMCID: PMC10018954.
28. Gittings LM, Alsop EB, Antone J, Singer M, Whitsett TG, Sattler R, Van Keuren-Jensen K. Cryptic exon detection and transcriptomic changes revealed in single-nuclei RNA sequencing of C9ORF72 patients spanning the ALS-FTD spectrum. Acta Neuropathol. 2023;146(3):433-50. Epub 20230719. doi: 10.1007/s00401-023-02599-5. PubMed PMID: 37466726; PMCID: PMC10412668.
29. Cao MC, Ryan B, Wu J, Curtis MA, Faull RLM, Dragunow M, Scotter EL. A panel of TDP-43-regulated splicing events verifies loss of TDP-43 function in amyotrophic lateral sclerosis brain tissue. Neurobiol Dis. 2023;185:106245. Epub 20230730. doi: 10.1016/j.nbd.2023.106245. PubMed PMID: 37527763.
30. Brown AL, Wilkins OG, Keuss MJ, Hill SE, Zanovello M, Lee WC, Bampton A, Lee FCY, Masino L, Qi YA, Bryce-Smith S, Gatt A, Hallegger M, Fagegaltier D, Phatnani H, Consortium NA, Newcombe J, Gustavsson EK, Seddighi S, Reyes JF, Coon SL, Ramos D, Schiavo G, Fisher EMC, Raj T, Secrier M, Lashley T, Ule J, Buratti E, Humphrey J, Ward ME, Fratta P. TDP-43 loss and ALS-risk SNPs drive mis-splicing and depletion of UNC13A. Nature. 2022;603(7899):131-7. Epub 20220223. doi: 10.1038/s41586-022-04436-3. PubMed PMID: 35197628; PMCID: PMC8891020.
31. Seddighi S, Qi YA, Brown AL, Wilkins OG, Bereda C, Belair C, Zhang YJ, Prudencio M, Keuss MJ, Khandeshi A, Pickles S, Kargbo-Hill SE, Hawrot J, Ramos DM, Yuan H, Roberts J, Sacramento EK, Shah SI, Nalls MA, Colon-Mercado JM, Reyes JF, Ryan VH, Nelson MP, Cook CN, Li Z, Screven L, Kwan JY, Mehta PR, Zanovello M, Hallegger M, Shantaraman A, Ping L, Koike Y, Oskarsson B, Staff NP, Duong DM, Ahmed A, Secrier M, Ule J, Jacobson S, Reich DS, Rohrer JD, Malaspina A, Dickson DW, Glass JD, Ori A, Seyfried NT, Maragkakis M, Petrucelli L, Fratta P, Ward ME. Mis-spliced transcripts generate de novo proteins in TDP-43-related ALS/FTD. Sci Transl Med. 2024;16(734):eadg7162. Epub 20240214. doi: 10.1126/scitranslmed.adg7162. PubMed PMID: 38277467; PMCID: PMC11325748.
32. Ruijtenberg S, Hoek TA, Yan X, Tanenbaum ME. Imaging Translation Dynamics of Single mRNA Molecules in Live Cells. Methods Mol Biol. 2018;1649:385-404. doi: 10.1007/978-1-4939-7213-5_26. PubMed PMID: 29130212.
33. Snouwaert JN, Church RJ, Jania L, Nguyen M, Wheeler ML, Saintsing A, Mieczkowski P, Manuel de Villena FP, Armao D, Moy SS, Lorenzo DN, Koller BH. A Mutation in the Borcs7 Subunit of the Lysosome Regulatory BORC Complex Results in Motor Deficits and Dystrophic Axonopathy in Mice. Cell Rep. 2018;24(5):1254-65. doi: 10.1016/j.celrep.2018.06.118. PubMed PMID: 30067980.
34. De Pace R, Britt DJ, Mercurio J, Foster AM, Djavaherian L, Hoffmann V, Abebe D, Bonifacino JS. Synaptic Vesicle Precursors and Lysosomes Are Transported by Different Mechanisms in the Axon of Mammalian Neurons. Cell Rep. 2020;31(11):107775. doi: 10.1016/j.celrep.2020.107775. PubMed PMID: 32553155; PMCID: PMC7478246.
35. Farfel-Becker T, Roney JC, Cheng XT, Li S, Cuddy SR, Sheng ZH. Neuronal Soma-Derived Degradative Lysosomes Are Continuously Delivered to Distal Axons to Maintain Local Degradation Capacity. Cell Rep. 2019;28(1):51-64 e4. doi: 10.1016/j.celrep.2019.06.013. PubMed PMID: 31269450; PMCID: PMC6696943.

36. Nicolas A, Kenna KP, Renton AE, Ticozzi N, Faghri F, Chia R, Dominov JA, Kenna BJ, Nalls MA, Keagle P, Rivera AM, van Rheenen W, Murphy NA, van Vugt J, Geiger JT, Van der Spek RA, Pliner HA, Shankaracharya, Smith BN, Marangi G, Topp SD, Abramzon Y, Gkazi AS, Eicher JD, Kenna A, Consortium I, Mora G, Calvo A, Mazzini L, Riva N, Mandrioli J, Caponnetto C, Battistini S, Volanti P, La Bella V, Conforti FL, Borghero G, Messina S, Simone IL, Trojsi F, Salvi F, Logullo FO, D'Alfonso S, Corrado L, Capasso M, Ferrucci L, Genomic Translation for ALSCC, Moreno CAM, Kamalakaran S, Goldstein DB, Consortium ALSS, Gitler AD, Harris T, Myers RM, Consortium NA, Phatnani H, Musunuri RL, Evani US, Abhyankar A, Zody MC, Answer ALSF, Kaye J, Finkbeiner S, Wyman SK, LeNail A, Lima L, Fraenkel E, Svendsen CN, Thompson LM, Van Eyk JE, Berry JD, Miller TM, Kolb SJ, Cudkowicz M, Baxi E, Clinical Research in ALS, Related Disorders for Therapeutic Development C, Benatar M, Taylor JP, Rampersaud E, Wu G, Wuu J, Consortium S, Lauria G, Verde F, Fogh I, Tiloca C, Comi GP, Soraru G, Cereda C, French ALSC, Corcia P, Laaksovirta H, Myllykangas L, Jansson L, Valori M, Ealing J, Hamdalla H, Rollinson S, Pickering-Brown S, Orrell RW, Sidle KC, Malaspina A, Hardy J, Singleton AB, Johnson JO, Arepalli S, Sapp PC, McKenna-Yasek D, Polak M, Asress S, Al-Sarraj S, King A, Troakes C, Vance C, de Belleroche J, Baas F, Ten Asbroek A, Munoz-Blanco JL, Hernandez DG, Ding J, Gibbs JR, Scholz SW, Floeter MK, Campbell RH, Landi F, Bowser R, Pulst SM, Ravits JM, MacGowan DJL, Kirby J, Pioro EP, Pamphlett R, Broach J, Gerhard G, Dunckley TL, Brady CB, Kowall NW, Troncoso JC, Le Ber I, Mouzat K, Lumbroso S, Heiman-Patterson TD, Kamel F, Van Den Bosch L, Baloh RH, Strom TM, Meitinger T, Shatunov A, Van Eijk KR, de Carvalho M, Kooyman M, Middelkoop B, Moisse M, McLaughlin RL, Van Es MA, Weber M, Boylan KB, Van Blitterswijk M, Rademakers R, Morrison KE, Basak AN, Mora JS, Drory VE, Shaw PJ, Turner MR, Talbot K, Hardiman O, Williams KL, Fifita JA, Nicholson GA, Blair IP, Rouleau GA, Esteban-Perez J, Garcia-Redondo A, Al-Chalabi A, Project Min EALSSC, Rogaeva E, Zinman L, Ostrow LW, Maragakis NJ, Rothstein JD, Simmons Z, Cooper-Knock J, Brice A, Goutman SA, Feldman EL, Gibson SB, Taroni F, Ratti A, Gellera C, Van Damme P, Robberecht W, Fratta P, Sabatelli M, Lunetta C, Ludolph AC, Andersen PM, Weishaupt JH, Camu W, Trojanowski JQ, Van Deerlin VM, Brown RH, Jr., van den Berg LH, Veldink JH, Harms MB, Glass JD, Stone DJ, Tienari P, Silani V, Chio A, Shaw CE, Traynor BJ, Landers JE. Genome-wide Analyses Identify KIF5A as a Novel ALS Gene. Neuron. 2018;97(6):1267-88. doi: 10.1016/j.neuron.2018.02.027. PubMed PMID: 29566793; PMCID: PMC5867896.
37. De Pace R, Maroofian R, Paimboeuf A, Zamani M, Zaki MS, Sadeghian S, Azizimalamiri R, Galehdari H, Zeighami J, Williamson CD, Fleming E, Zhou D, Gannon JL, Thiffault I, Roze E, Suri M, Zifarelli G, Bauer P, Houlden H, Severino M, Patten SA, Farrow E, Bonifacino JS. Biallelic BORCS8 variants cause an infantile-onset neurodegenerative disorder with altered lysosome dynamics. Brain. 2024;147(5):1751-67. doi: 10.1093/brain/awad427. PubMed PMID: 38128568; PMCID: PMC11068110.
38. Yang C, Wang H, Qiao T, Yang B, Aliaga L, Qiu L, Tan W, Salameh J, McKenna-Yasek DM, Smith T, Peng L, Moore MJ, Brown RH, Jr., Cai H, Xu Z. Partial loss of TDP-43 function causes phenotypes of amyotrophic lateral sclerosis. Proc Natl Acad Sci U S A. 2014;111(12):E1121-9. Epub 20140310. doi: 10.1073/pnas.1322641111. PubMed PMID: 24616503; PMCID: PMC3970502.
39. Lee EB, Lee VM, Trojanowski JQ. Gains or losses: molecular mechanisms of TDP43-mediated neurodegeneration. Nat Rev Neurosci. 2011;13(1):38-50. Epub 20111130. doi: 10.1038/nrn3121. PubMed PMID: 22127299; PMCID: PMC3285250.
40. Fernandopulle MS, Prestil R, Grunseich C, Wang C, Gan L, Ward ME. Transcription Factor-Mediated Differentiation of Human iPSCs into Neurons. Curr Protoc Cell Biol. 2018;79(1):e51. Epub 20180518. doi: 10.1002/cpcb.51. PubMed PMID: 29924488; PMCID: PMC6993937.

41. Wang C, Ward ME, Chen R, Liu K, Tracy TE, Chen X, Xie M, Sohn PD, Ludwig C, Meyer-Franke A, Karch CM, Ding S, Gan L. Scalable Production of iPSC-Derived Human Neurons to Identify Tau-Lowering Compounds by High-Content Screening. Stem Cell Reports. 2017;9(4):1221-33. Epub 20170928. doi: 10.1016/j.stemcr.2017.08.019. PubMed PMID: 28966121; PMCID: PMC5639430.
42. Wang B, Wang M, Zhang W, Xiao T, Chen CH, Wu A, Wu F, Traugh N, Wang X, Li Z, Mei S, Cui Y, Shi S, Lipp JJ, Hinterndorfer M, Zuber J, Brown M, Li W, Liu XS. Integrative analysis of pooled CRISPR genetic screens using MAGeCKFlute. Nat Protoc. 2019;14(3):756-80. Epub 20190201. doi: 10.1038/s41596-018-0113-7. PubMed PMID: 30710114; PMCID: PMC6862721.
43. Carpenter AE, Jones TR, Lamprecht MR, Clarke C, Kang IH, Friman O, Guertin DA, Chang JH, Lindquist RA, Moffat J, Golland P, Sabatini DM. CellProfiler: image analysis software for identifying and quantifying cell phenotypes. Genome Biol. 2006;7(10):R100. Epub 20061031. doi: 10.1186/gb-2006-7-10-r100. PubMed PMID: 17076895; PMCID: PMC1794559.
44. Livak KJ, Schmittgen TD. Analysis of relative gene expression data using real-time quantitative PCR and the 2(-Delta Delta C(T)) Method. Methods. 2001;25(4):402-8. doi: 10.1006/meth.2001.1262. PubMed PMID: 11846609.
45. Dobin A, Davis CA, Schlesinger F, Drenkow J, Zaleski C, Jha S, Batut P, Chaisson M, Gingeras TR. STAR: ultrafast universal RNA-seq aligner. Bioinformatics. 2013;29(1):15-21. Epub 20121025. doi: 10.1093/bioinformatics/bts635. PubMed PMID: 23104886; PMCID: PMC3530905.
46. Vaquero-Garcia J, Barrera A, Gazzara MR, Gonzalez-Vallinas J, Lahens NF, Hogenesch JB, Lynch KW, Barash Y. A new view of transcriptome complexity and regulation through the lens of local splicing variations. Elife. 2016;5:e11752. Epub 20160201. doi: 10.7554/eLife.11752. PubMed PMID: 26829591; PMCID: PMC4801060.
47. Molder F, Jablonski KP, Letcher B, Hall MB, Tomkins-Tinch CH, Sochat V, Forster J, Lee S, Twardziok SO, Kanitz A, Wilm A, Holtgrewe M, Rahmann S, Nahnsen S, Koster J. Sustainable data analysis with Snakemake. F1000Res. 2021;10:33. Epub 20210118. doi: 10.12688/f1000research.29032.2. PubMed PMID: 34035898; PMCID: PMC8114187.
48. Reilly L, Lara E, Ramos D, Li Z, Pantazis CB, Stadler J, Santiana M, Roberts J, Faghri F, Hao Y, Nalls MA, Narayan P, Liu Y, Singleton AB, Cookson MR, Ward ME, Qi YA. A fully automated FAIMS-DIA mass spectrometry-based proteomic pipeline. Cell Rep Methods. 2023;3(10):100593. Epub 20230919. doi: 10.1016/j.crmeth.2023.100593. PubMed PMID: 37729920; PMCID: PMC10626189.
49. Cox J, Mann M. MaxQuant enables high peptide identification rates, individualized p.p.b.-range mass accuracies and proteome-wide protein quantification. Nat Biotechnol. 2008;26(12):1367-72. Epub 20081130. doi: 10.1038/nbt.1511. PubMed PMID: 19029910.
50. Frankenfield AM, Ni J, Ahmed M, Hao L. Protein Contaminants Matter: Building Universal Protein Contaminant Libraries for DDA and DIA Proteomics. J Proteome Res. 2022;21(9):2104-13. Epub 20220706. doi: 10.1021/acs.jproteome.2c00145. PubMed PMID: 35793413; PMCID: PMC10040255.
51. Hasan S, Fernandopulle MS, Humble SW, Frankenfield AM, Li H, Prestil R, Johnson KR, Ryan BJ, Wade-Martins R, Ward ME, Hao L. Multi-modal proteomic characterization of lysosomal function and proteostasis in progranulin-deficient neurons. Mol Neurodegener. 2023;18(1):87. Epub 20231116. doi: 10.1186/s13024-023-00673-w. PubMed PMID: 37974165; PMCID: PMC10655356.

Figures and legends

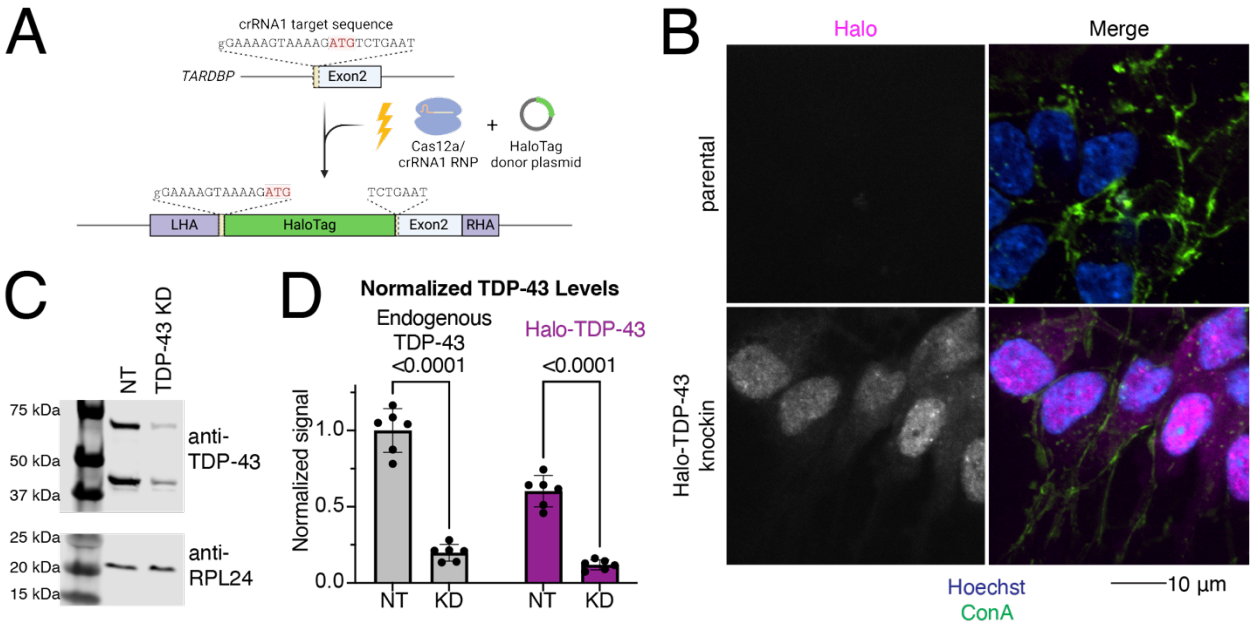

Figure 1: Generation of an endogenously HaloTagged TDP-43 iPSC line.

A) Schematic of knock in to N-terminus of TDP-43. Cas12a-crRNA ribonucleoparticle (RNP) and HaloTag donor plasmid containing homology arms to TDP-43 were nucleofected into iPSCs. Halo was knocked in to a single TDP-43 allele at the N-terminus of the protein, before exon 2.

B) Microscopy validation of Halo-TDP-43 localization to nucleus. Halo in pink, ConA lipid dye in green, and Hoechst in blue. Scale bar 10 µm.

C) TDP-43 western blot of NT and TDP-43 KD neurons. Halo-TDP-43 is approximately 33 kDa heavier than untagged TDP-43, which corresponds to the molecular weight of Halo. RPL24 is shown as a loading control. TDP-43 KD decreases levels of both tagged and untagged TDP-43.

D) Quantification of western blot shown in (C) shows untagged (left) and Halo-Tagged (right) TDP-43 is decreased upon TDP-43 KD. Interestingly, Halo-TDP-43 is expressed at levels about one half as much as untagged TDP-43.

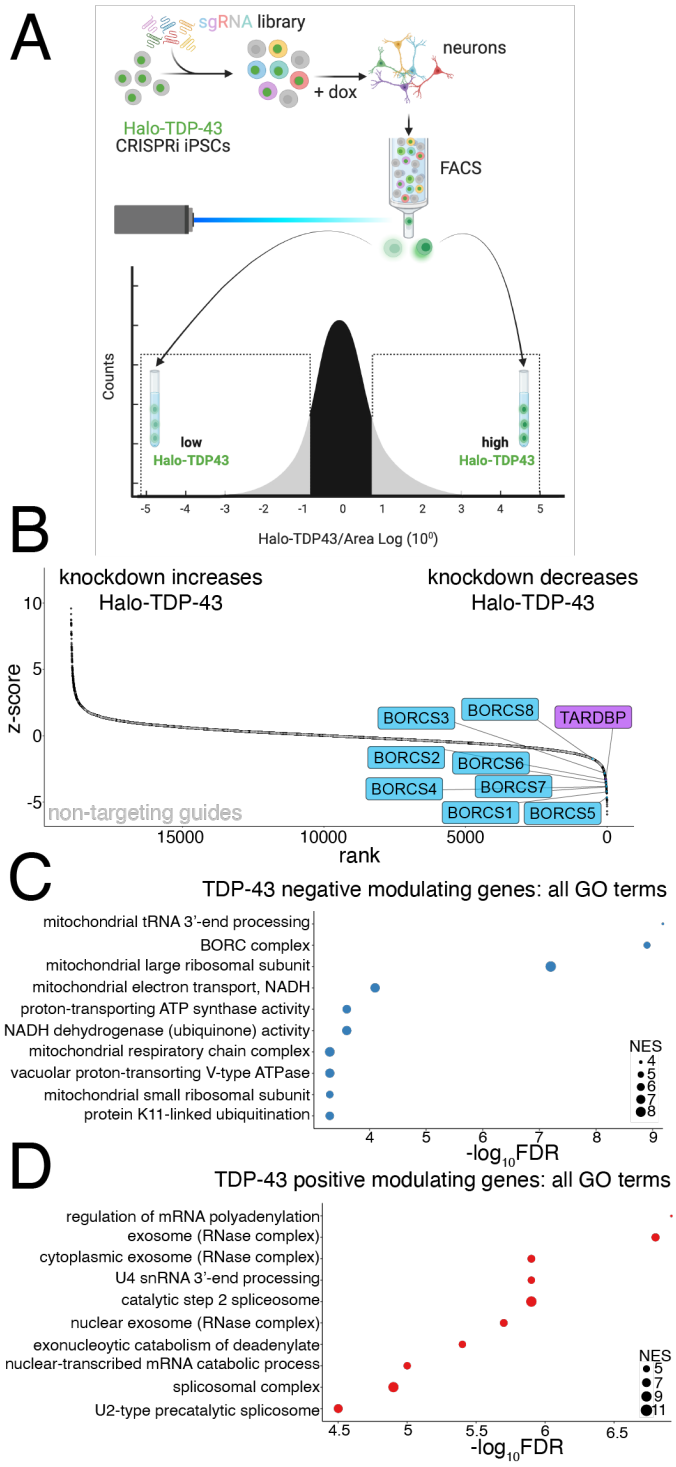

Figure 2: CRISPRi screen identifies modifiers of TDP-43 protein levels in iPSC-derived neurons.

A) Schematic of FACS screen. Halo-TDP-43 iPSCs were transduced with the dual guide library and selected. After selection, iPSCs were differentiated to neurons via Dox-inducible NGN2 expression. Neurons were FACS sorted and populations expressing high Halo-TDP-43 and low Halo-TDP-43 were collected, DNA extracted, and sgRNA libraries sequenced.

B) Rank plot of screen results showing genes whose KD increases Halo-TDP-43 levels (left) and genes whose KD decreases Halo-TDP-43 levels, including TDP-43 itself (right). BORC genes are in blue.

C) GO analysis of screen hits that reduce Halo-TDP-43 levels include the BORC complex and many mitochondria-associated terms. The FDR is from the calculated permutation p value of 1000 iterations.

D) GO analysis of screen hits that increase Halo-TDP-43 levels include many hits related to mRNA processing. The FDR is from the calculated permutation p value of 1000 iterations.

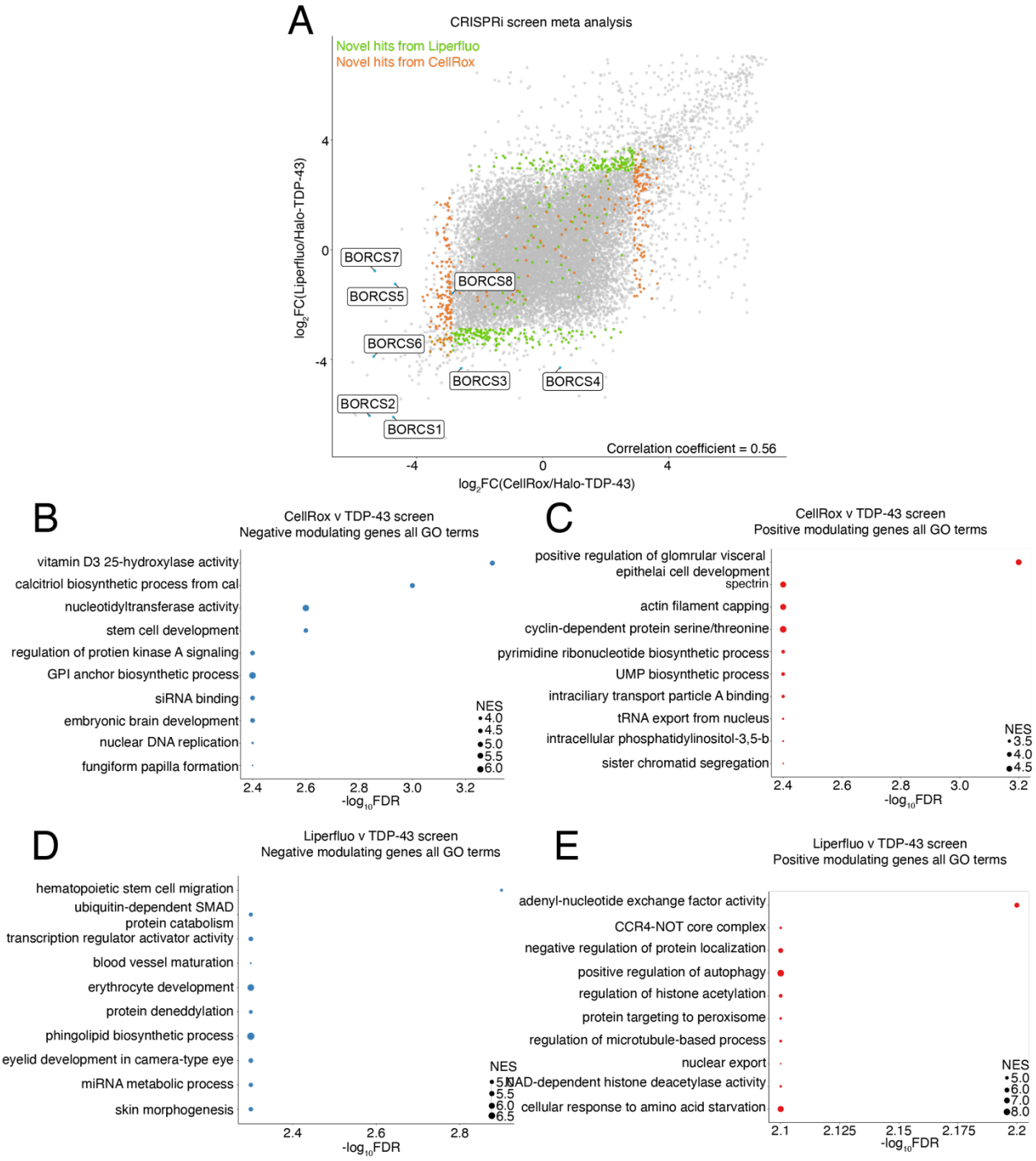

Figure 3: Meta-analysis of CRISPRi screens identifies novel and common genes.

A) Comparison of CellRox/Halo-TDP-43 meta-analysis to Liperfluo/Halo-TDP-43 meta-analysis shows many genes lie close to a line with a slope of one, demonstrating that many genes change levels of various readouts in similar ways. R value = 0.56. BORC genes are highlighted in blue, novel hits from Liperfluo and CellRox screens as compared to our Halo-TDP-43 screen are indicated in green and orange, respectively.
B) GO analysis of genes that negatively modulate readouts for CellRox and Halo-TDP-43 screens show DNA and signaling related terms. The FDR is from the calculated permutation p value of 1000 iterations.
C) GO analysis of genes that positively modulate readouts for CellRox and Halo-TDP-43 screens show translation related terms. The FDR is from the calculated permutation p value of 1000 iterations.
D) GO analysis of genes that negatively modulate readouts for Liperfluo and Halo-TDP-43 screens show terms related to ubiquitination, neddylation, and lipids. The FDR is from the calculated permutation p value of 1000 iterations.
E) GO analysis of genes that positively modulate readouts for Liperfluo and Halo-TDP-43 screens show adenosine, acetylation, and autophagy related terms. The FDR is from the calculated permutation p value of 1000 iterations.

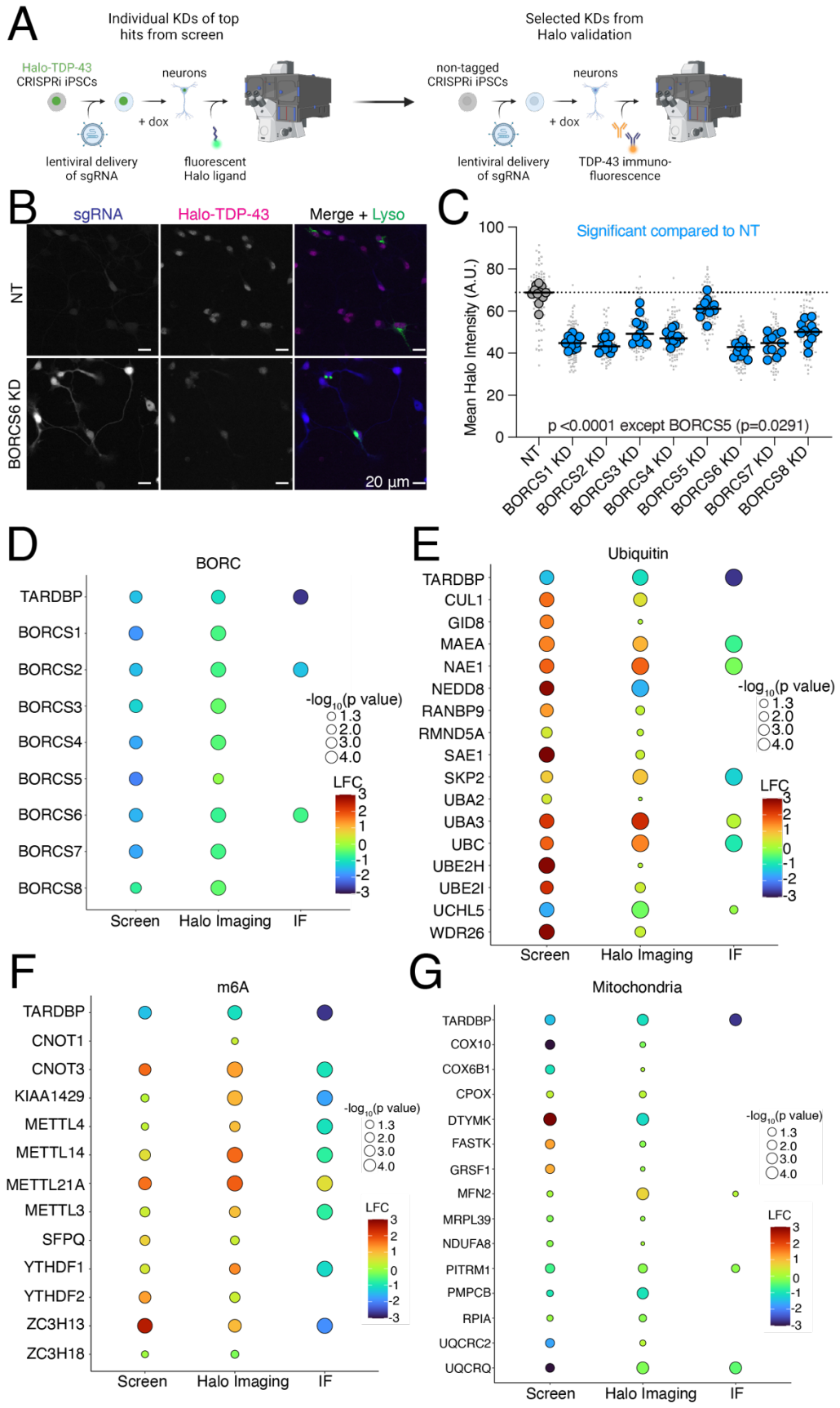
A
Individual KDs of top hits from screen
Halo-TDP-43 CRISPRi iPSCs
neurons
+ dox
lentiviral delivery of sgRNA
fluorescent Halo ligand
Selected KDs from Halo validation
non-tagged CRISPRi iPSCs
neurons
+ dox
lentiviral delivery of sgRNA
TDP-43 immuno-fluorescence
B
sgRNA
Halo-TDP-43
Merge + Lyso
NT
BORCS6 KD
20 µm
C
Significant compared to NT
Mean Halo Intensity (A.U.)
p <0.0001 except BORCS5 (p=0.0291)
NT
BORCS1 KD
BORCS2 KD
BORCS3 KD
BORCS4 KD
BORCS5 KD
BORCS6 KD
BORCS7 KD
BORCS8 KD
D
BORC
TARDBP
BORCS1
BORCS2
BORCS3
BORCS4
BORCS5
BORCS6
BORCS7
BORCS8
Screen
Halo Imaging
IF
-log10(p value)
LFC
E
Ubiquitin
TARDBP
CUL1
GID8
MAEA
NAE1
NEDD8
RANBP9
RMND5A
SAE1
SKP2
UBA2
UBA3
UBC
UBE2H
UBE2I
UCHL5
WDR26
Screen
Halo Imaging
IF
-log10(p value)
LFC
F
m6A
TARDBP
CNOT1
CNOT3
KIAA1429
METTL4
METTL14
METTL21A
METTL3
SFPQ
YTHDF1
YTHDF2
ZC3H13
ZC3H18
Screen
Halo Imaging
IF
-log10(p value)
LFC
G
Mitochondria
TARDBP
COX10
COX6B1
CPOX
DTYMK
FASTK
GRSF1
MFN2
MRPL39
NDUFA8
PITRM1
PMPCB
RPIA
UQCRC2
UQCRQ
Screen
Halo Imaging
IF
-log10(p value)
LFC

Figure 4: Validation of modulators of TDP-43 levels in iPSC-derived neurons.

A) Schematic of hit validation. As a first validation, Halo-TDP-43 iPSCs were transduced with single sgRNAs against hit genes and Halo levels were analyzed by microscopy, generating a list of Halo-validated hits. Then some genes were selected from the Halo-validated hits and untagged iPSCs were transduced with the same virus and TDP-43 protein levels assessed via TDP-43 immunofluorescence microscopy, identifying hits not affected by a HaloTag.
B) Representative images of Halo-TDP-43 live cell imaging with BORCS6 KD. sgRNA plasmids contain a cytoplasmic BFP, enabling identification of cells expressing the sgRNA. For BORC genes, iPSCs were transduced with a lysosome marker (LAMP1-mApple) to ensure functional BORC KD through depletion of neuritic lysosomes. Scale bar represents 20 µm.
C) Quantification of BORC KD Halo-TDP-43 microscopy. All BORC genes tested (S1-S8) showed statistically significant decreases in Halo-TDP-43 levels compared to a non-targeting (NT) guide, indicated by blue dots. N=12 wells per genotype, 9 images per well (small gray dots). Significant p-values indicated on graph.
D) (D-G) Summary graphs of screen, Halo live cell imaging, and TDP-43 immunofluorescence imaging fold changes for D) BORC KD,
E) E) Ubiquitin-associated gene KD,
F) F) m6A-associated gene KD, and
G) G) mitochondria gene KDs. Color indicates strength of $\log_2$FoldChange for each condition, circle size indicates $-\log_{10}$p-value; values below 1.3 are not significant, corresponding to a p-value of 0.05. No circle indicates the gene was not tested in that experiment (i.e., not all genes were tested by immunofluorescence).

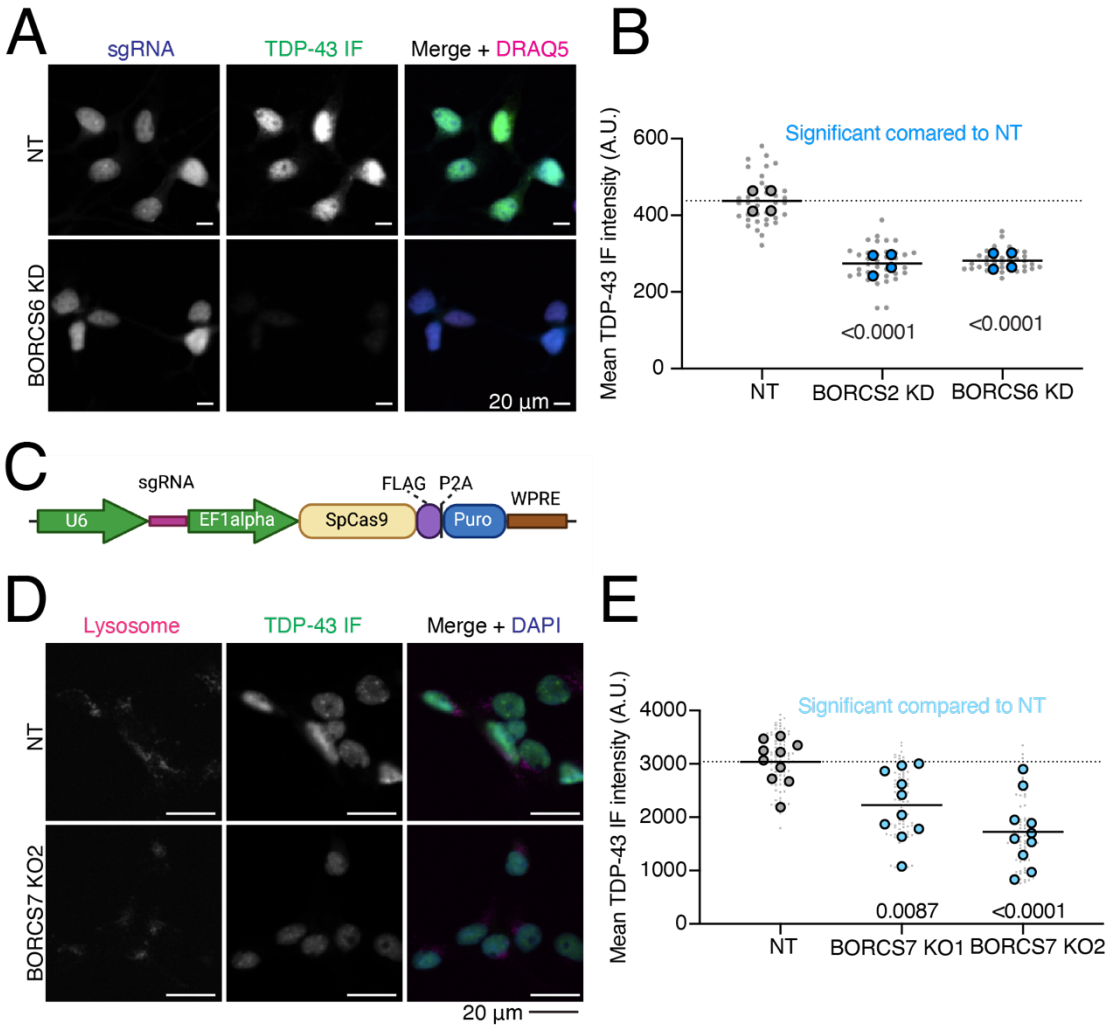

Figure 5: Endogenous validation of TDP-43 level modifiers in iPSC-derived neurons.

A) Quantification of BORC KD TDP-43 immunofluorescence microscopy. Both BORC genes tested (S2 and S6) show significant decreases in untagged TDP-43 levels compared to a NT guide, indicated by blue dots. N=4 wells per genotype, 9 images per well (small gray dots). Significant p-values indicated on graph.
B) Representative images of TDP-43 immunofluorescence imaging with BORCS6 KD. sgRNA plasmids contain a cytoplasmic BFP, enabling identification of cells expressing the sgRNA. Scale bar represents 20 µm.
C) Schematic of pLentiCRISPR plasmid. pLentiCRISPR enables lentiviral delivery of a plasmid expressing an sgRNA of interest under a U6 promoter and Cas9 under an Ef1alpha promoter. This enables knockout of a gene of interest targeted by an sgRNA.
D) Representative images of BORCS7 KO TDP-43 IF with lysosomes stained with anti-H4A3 antibody. Scale bar is 20 µm.
E) Quantification of TDP-43 immunofluorescence on BORCS7 knockout neurons. Both BORCS7 guides significantly reduced the amount of TDP-43 IF signal compared to a NT guide, light blue dots. N=10 wells, 9 images per well (light gray dots). Significant p-values indicated on graph.

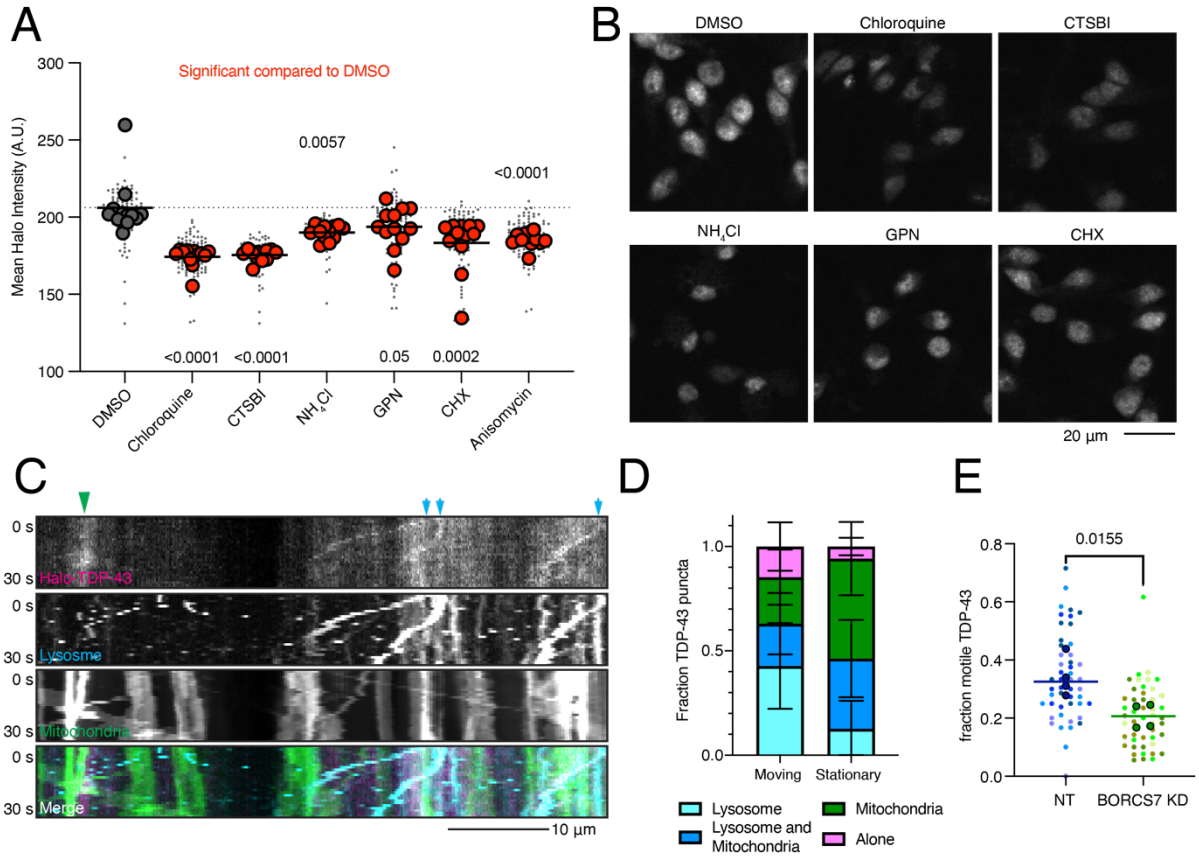

Figure 6: TDP-43 protein levels require active and neuritically localized lysosomes.

A) Drugs targeting different aspects of lysosome function decrease Halo-TDP-43 levels. All drugs tested were significant compared to a DMSO treatment, indicated by red dots. N=12 wells, 9 images per well (small grey dots), mean of each well is indicated by large dot.

B) Representative images of drug treatments that decrease Halo-TDP-43 levels. Scale bar is 20 µm.

C) Representative 30 s kymographs of Halo-TDP-43, lysosomes (LAMP1-mApple), mitochondria (mito-mEmerald), showing co-transport of Halo-TDP-43 with organelles. Green arrowhead indicates co-localization with static mitochondria; blue arrows indicate co-localization with motile lysosomes. Scale bar is 10 µm.

D) Quantification of Halo-TDP-43 signal with organelles. Motile Halo-TDP-43 in neurites is primarily co-transported with lysosomes or lysosomes and mitochondria together. Stationary Halo-TDP-43 is more likely to be associated with mitochondria.

E) Upon BORCS7 KD, TDP-43 is less mobile compared to a NT guide, likely due to restriction of lysosomes to the soma. N=4 wells (mean per well indicated by large dot), 8 images per well (small dots).

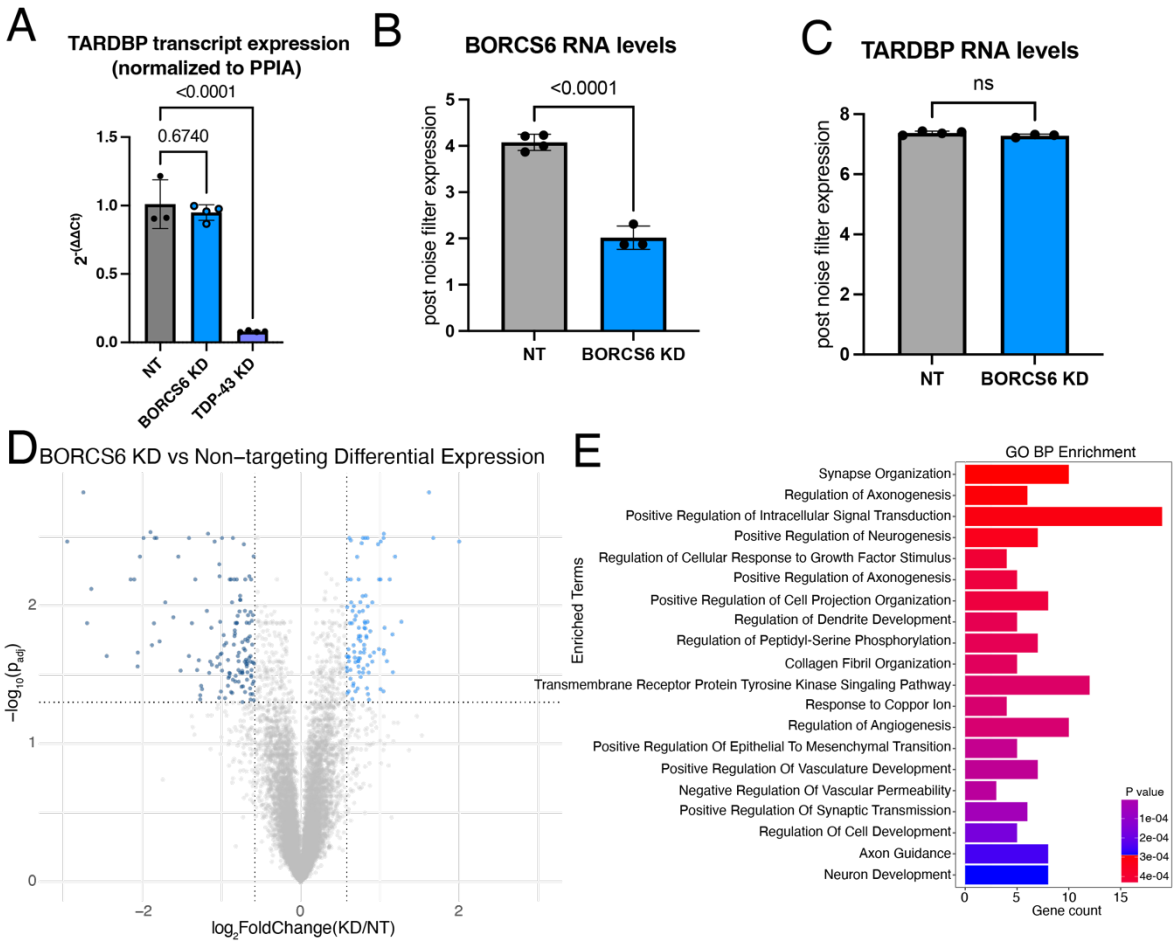

Figure 7: BORC KD does not affect TDP-43 RNA levels.

A) qPCR of NT, BORCS6 KD, and TDP-43 KD neurons showing decreased TDP-43 mRNA levels in TDP-43 KD, but not BORCS6 KD. Normalized to PPIA. NT n=3, BORCS6 KD n=4, and TDP-43 KD n=4.
B) Normalized transcript counts of NT and BORCS6 KD neurons showing about half as much BORCS6 mRNA in BORCS6 KD neurons. NT n=4, BORCS6 KD n=3.
C) Normalized transcript counts of NT and BORCS6 KD neurons showing no change in TARDBP (TDP-43) mRNA levels in BORCS6 KD neurons. NT n=4, BORCS6 KD n=3.
D) Volcano plot comparing BORCS6 KD with NT neurons. 98 genes increase expression upon BORCS6 KD (right of graph), while 139 genes decrease expression (left of graph). NT n=4, BORCS6 KD n=3.
E) GO BP enrichment analysis from Enrichr of genes significantly altered in BORCS6 KD neurons compared to NT neurons shows several neuron and axon related terms.

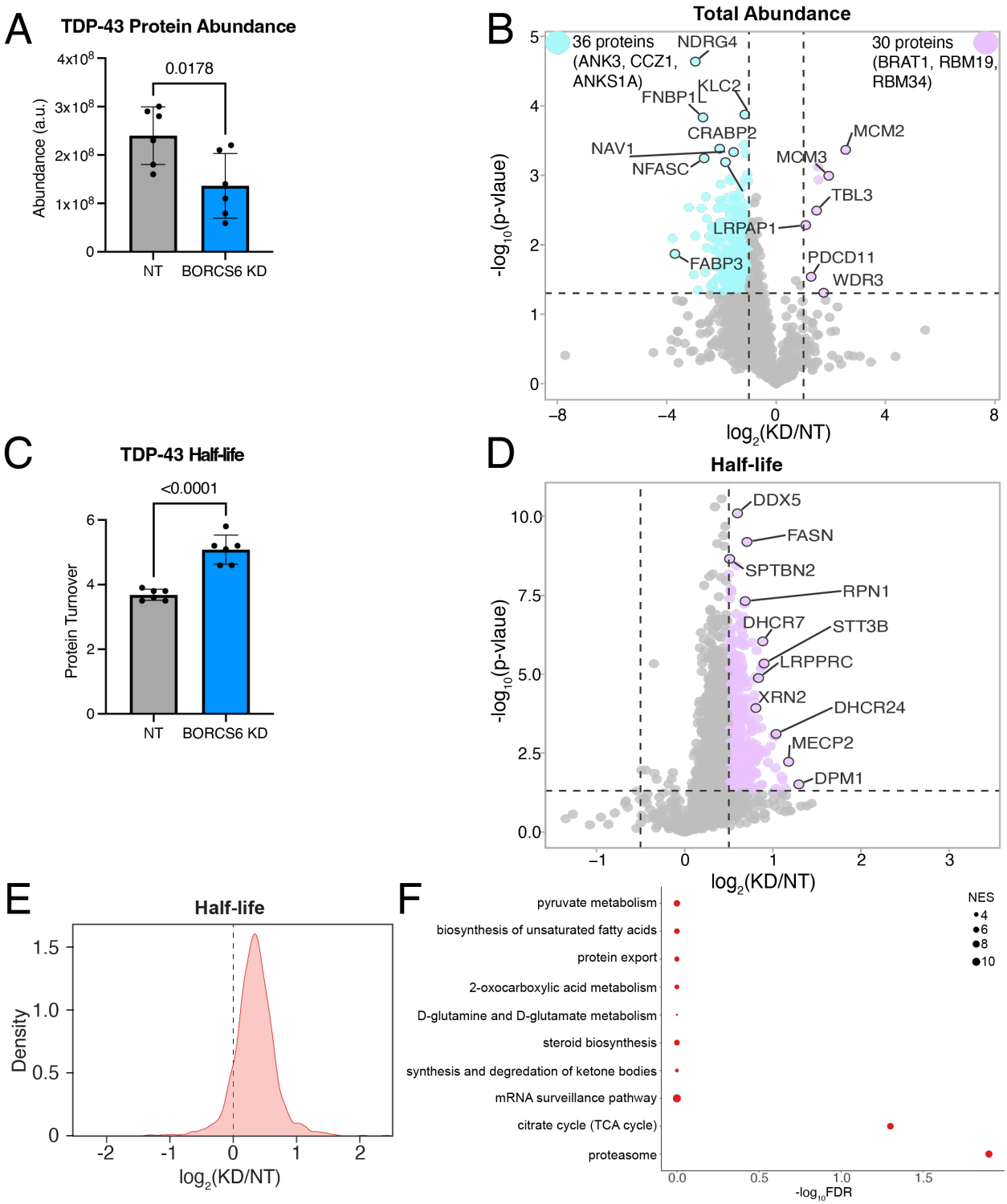

Figure 8: BORC KD alters the abundance and half-lives of TDP-43 and other proteins.

A) TDP-43 protein has decreased total abundance in day 7 BORCS6 neurons.

B) Volcano plot of total protein abundance comparing BORCS6 KD to a non-targeting guide. Some proteins (purple) have increased abundance, while a larger number (teal) have decreased abundance. Non-significant or low $\log_2$(fold change) proteins are

indicated in grey. Vertical lines at log_2(fold change) of 1 and -1, horizontal line at p-value = 0.05.

C) TDP-43 has longer half-life in day 7 BORCS6 KD neurons.

D) Volcano plot of half-life changes in BORCS6 KD neurons as compared to neurons expressing a non-targeting guide. Non-significant or low log_2(fold change) protein turnovers are indicated in grey. Horizontal line at p=0.05, vertical lines at log_2(fold change) of 0.5 or -0.5.

E) Density plot of global protein turnover shows longer protein half-lives upon BORC KD.

F) Gene ontology enrichment analysis using proteins with longer half-lives in BORCS6 KD neurons shows KEGG pathways related to protein export, proteasome, and metabolism.